Path instabilities of a freely rising or falling sphere

Raaghav, Shravan K.R.; Poelma, Christian; Breugem, Wim Paul

DOI
10.1016/j.ijmultiphaseflow.2022.104111

Publication date
2022

Document Version
Final published version

Published in
International Journal of Multiphase Flow

International Journal of Multiphase Flow 153 (2022) 104111

Contents lists available at ScienceDirect

International Journal of Multiphase Flow

journal homepage: www.elsevier.com/locate/ijmulflow

Path instabilities of a freely rising or falling sphere

Shravan K.R. Raaghav, Christian Poelma, Wim-Paul Breugem *

Laboratory for Aero & Hydrodynamics, Process & Energy Department, Delft University of Technology, Mekelweg 2, 2628 CD Delft, The Netherlands

ARTICLE INFO

Keywords:
Freely rising/falling sphere
Path instability
Wake instability
Regime map
Particle tracking velocimetry

ABSTRACT

Path instabilities of a sphere rising or falling in a quiescent Newtonian fluid have been studied experimentally. The rich palette of possible instabilities is dependent upon two dimensionless quantities, namely the Galileo number (Ga) and the particle/fluid mass density ratio ($\overline{\rho}$). In recent literature, several ($Ga, \overline{\rho}$) regime maps have been proposed to characterize path instabilities, based on both numerical and experimental studies, with substantial disagreements among them. The present study attempts to shed light on path instabilities for which previous studies disagree. A detailed experimental investigation has been conducted for 219 different combinations of Ga and $\overline{\rho}$, grouped around four values of $\overline{\rho}$ ($\sim$ 0.87, 1.12, 3.19 and 3.9) and Ga in the range of $\sim$ 100 to 700. Our results agree well with literature for the low Ga range in which a particle takes a steady vertical or steady oblique path and for which all previous studies agree with each other. For the higher and more controversial Ga range, we discuss consensus and disagreements with previous studies. Some regimes, which were only recently observed in numerical simulations, have been observed experimentally for the first time. Also, intriguing bi-stable regimes (i.e., coexistence of two stable asymptotic states) have been observed. For all four investigated density ratios, an update of the regime map is proposed. Finally, for both the rising and falling spheres, the drag coefficient as function of terminal settling Reynolds number has been determined, which for the investigated density ratios does not differ significantly from that of flow past a fixed sphere.

1. Introduction

Studying the dynamics of rising and falling spheres in a quiescent fluid is crucial for understanding many transport phenomena in dispersed multiphase flows. Particle-laden flows occur in many natural processes like in geophysical/atmospheric flows and the settling of micro-organisms (plankton) and as such are ubiquitous part of life. Particle-laden flows are also found in widespread industrial applications including spray drying, cyclone separators, fluidized bed reactors, paper manufacturing and water treatment plants. Although the research on a freely falling or rising sphere in a fluid spans more than three centuries since the pioneering work by Newton (1726), the present understanding is far from complete (Ern et al., 2012).

Unlike the freely moving sphere, the flow regimes and wake dynamics of a fixed sphere have been extensively studied, both numerically and experimentally, and the understanding is quite clear (Ghidersa and Dušek, 2000; Mittal, 1999; Natarajan and Acrivos, 1993; Ormières and Provansal, 1999; Tomboulides and Orszag, 2000; Fabre et al., 2008). The scenario of a freely moving sphere has received comparatively less attention. The six additional degrees of freedom for translation and rotation lead to different path and wake instabilities resulting in a variety of path characteristics, which are reminiscent of typical paths observed for rising bubbles. The path instabilities are triggered via wake instabilities and wake-induced loads (Ern et al., 2012). For a settling or ascending homogeneous sphere in a still fluid, the entire dynamics of the path instabilities can be fully characterized by the particle/fluid mass density ratio and the Galileo number, which are defined by, respectively:

$$\overline{\rho} = \frac{\rho_p}{\rho_f}\,, \tag{1a}$$

$$Ga = \sqrt{\frac{|\,\overline{\rho} - 1\,|\, g d_p^3}{\nu_f^2}}\,, \tag{1b}$$

where ρ_p and ρ_f are the sphere and fluid densities, respectively, g is the gravitational acceleration, d_p is the sphere diameter and ν_f is the kinematic viscosity of the fluid. The Galileo number can be interpreted as the Reynolds number based on the inertio-gravitational velocity, $v_g = \sqrt{|\,\overline{\rho} - 1\,|\, g d_p}$.

Only fairly recently, thanks to the increase of the computational capabilities, Jenny et al. (2004) (hereinafter denoted as JDB) were the first to explore a wide range of the physical parameter space for the settling/ascension of a single sphere. Surprisingly, great richness in physics associated with different path and wake instabilities,

* Corresponding author.
E-mail address: w.p.breugem@tudelft.nl (W.-P. Breugem).

https://doi.org/10.1016/j.ijmultiphaseflow.2022.104111
Received 8 December 2021; Received in revised form 27 April 2022; Accepted 2 May 2022
Available online 19 May 2022

were observed. JDB observed six distinct regimes referred to as the steady vertical, steady oblique, low-frequency oscillating oblique, high-frequency oscillating oblique, low-frequency periodic zigzagging and chaotic regime. For all density ratios and sufficiently low Ga, the sphere moves steadily along a vertical path and exhibits an axisymmetric wake similar to the wake past a fixed sphere. This steady vertical regime was observed to undergo a first regular bifurcation at a Ga varying from around 155 to around 160 for very low and very high density ratio, respectively. This results in a steady oblique motion of the sphere in the presence of a steady angular velocity vector oriented in the horizontal plane and a slightly inclined plane-symmetric wake structure. It was reported in later studies that the critical Ga value is actually independent of the density ratio (as one may expect since the transition is from a steady to another steady regime) and located somewhere between 155–156 (Fabre et al., 2012; Zhou and Dušek, 2015), which corresponds to a critical Reynolds number slightly lower than the value of about 212 for the wake past a fixed sphere. Upon increasing Ga, the oblique sphere motion undergoes a secondary Hopf bifurcation leading to an oscillating oblique regime with periodic oscillations. The critical Ga for this bifurcation as well as the oscillation frequency were observed to depend on $\overline{\rho}$. Following the oscillating oblique regime, a periodic zigzagging regime was found for light spheres ($\overline{\rho} < 1$) for Ga in the range of 175–215. On the contrary, for heavy spheres ($\overline{\rho} > 1$) an immediate transition into chaotic motion was observed for Ga in the range of 210–230, with the sphere translating in the vertical on average (i.e., no mean drift) but with significant instantaneous 3D chaotic fluctuations in its motion. Following the periodic zigzagging regime for light spheres, JDB found a transition to the chaotic regime for Ga in the range of 185–215, but with the intriguing presence of a bi-stable regime for Ga in the range of 215–340. In this bi-stable regime, the asymptotic sphere behaviour corresponds either to a planar, vertical, small-amplitude and high-frequency oscillating state or to a chaotic state dependent of the initial condition.

A series of experimental studies followed the study of JDB. Veldhuis et al. (2004) and Veldhuis and Biesheuvel (2007) (hereinafter denoted as VB) primarily focused on verifying the intriguing results obtained by JDB. Particle trajectories were obtained from a high-speed camera using particle tracking and the wake structure was visualized using a Schlieren technique. Different combinations of Ga and $\overline{\rho}$ were investigated, probing each of the principal regimes identified by JDB (except the steady vertical regime). The steady oblique and the oscillating oblique regimes agreed quite well with the results of JDB. Although they were not able to observe a perfect zigzagging regime for light spheres, occasional zigzagging was observed, and they attributed this mismatch to a possible sphericity effect and/or inhomogeneity in mass distribution within the spheres. In a later study, they investigated the drag characteristics of light spheres (Veldhuis et al., 2009) (hereinafter denoted as VBL) and compared it to a fixed sphere. A strongly enhanced drag coefficient of about $C_d \simeq 0.85$ was found for $\overline{\rho} = 0.02$ and Re in the range of about 900–2000, associated with a zigzag or helicoidal path with large tangential velocity variations of the investigated spheres. On the contrary, experiments on moderately light and heavy spheres ($\overline{\rho}$ in the range of $\sim$ 0.85–2.6) did not show a significant deviation from the Turton–Levenspiel drag relation for a fixed sphere (Turton and Levenspiel, 1986).

Interestingly, an even more strongly enhanced drag coefficient for light spheres was reported earlier by Karamanev and co-workers based on experiments of rising spheres in water. Karamanev and Nikolov (1992) reported a constant C_d value of 0.95 for $\overline{\rho} < 0.3$ and $Re > 130$, related to the transition of vertical to spiralling sphere motion. In a later study, Karamanev et al. (1996) claimed the same constant C_d value of 0.95 for all $\left|\rho_p - \rho_f\right| d_p > 0.120$ g/cm^2, which boils down to $Re \gtrsim 175/\left|\overline{\rho} - 1\right|$ for their experiments in water at 25°C. This was reported for density ratios up to 0.99, which is in stark contrast with the findings of Veldhuis et al. (2009) for their moderately light and heavy spheres mentioned above.

Another, extensive, experimental study was conducted by Horowitz and Williamson (2010) (hereinafter denoted as HW). Based on 133 combinations of Re and $\overline{\rho}$, a new regime map was created; note that they used Re instead of Ga, but these numbers are related to each other according to $Re = Ga \cdot \sqrt{4/(3C_d)}$. Surprisingly, their findings were very different from the results from the above mentioned studies. Notably, for light spheres with a mass density ratio smaller than 0.36, a direct transition was reported from the steady oblique regime (between $Re \simeq$ 210–260) to a periodic zigzagging regime for $Re \gtrsim 260$ (corresponding to $Ga \gtrsim 190$) and which persisted up to the highest investigated Re (beyond 20,000). For density ratios larger than 0.36, the steady oblique regime transitions into an oblique regime with periodic ('R' mode) vortex shedding at $Re \simeq 270$ and this lasts till $Re \simeq 600$ (corresponding to $Ga \simeq 380$). For some regimes (e.g., zigzagging) new limits of Ga and $\overline{\rho}$ were proposed. Another striking finding was that the drag coefficient was $\simeq 0.75$ for all 'vibrating spheres', by which they meant all spheres displaying strong periodic (zigzagging) motion. This value was nearly independent of $\overline{\rho}$ and Re.

Motivated by the disagreements between the experiments of HW and the numerical simulations of JDB, the same research group of JDB recently performed numerical simulations with the goal to refine and extend their previous study to higher Ga in the chaotic regime (Zhou and Dušek, 2015, hereinafter denoted as ZD). Compared to JDB, they simulated the sphere motion for longer time intervals as to distinguish between chaotic behaviour with long transients of intermittent states (reminiscent of neighbouring, ordered, regimes) and truly bi-stable behaviour. Although most results did agree with their earlier study, ZD pointed out some corrections to the map that was proposed by JDB and updated the map (see Fig. 1). The zigzagging regime for light spheres was found to exist only for $\overline{\rho} \lesssim 0.5$ (vs $\lesssim 1$ in JDB). Also, the bi-stable regime identified by JDB, was found to be much smaller in extent as visible from the revised map (see the small spot around Ga = 250–260, to the left of the VO regime), underlining the importance to track the sphere motion over a sufficiently long time interval. Furthermore, the high-frequency vertical oscillating state was found to be the only stable asymptotic state for Ga and $\overline{\rho}$ in the range of, respectively, 250–300 and 0.5–2. Also, for $Ga \gtrsim 375$ and $\overline{\rho}$ near 0, a range not explored before by JDB, ZD found nearly perfect helical trajectories similar to the well-known spiralling trajectories of rising bubbles. Interestingly, for heavy spheres with $\overline{\rho} \gtrsim 1.7$ a more complex transition scenario to chaos was revealed, with the presence of a narrow Ga interval of 10–20 units with bi-stable behaviour located in between the high-frequency oscillating oblique and the three-dimensional chaotic regime. In this bi-stable regime the sphere behaviour is either in the chaotic state or the oscillating oblique state with possible slow co-rotation of the symmetry plane resulting in a helical trajectory. Finally, we note that also the new numerical results of ZD did not match well with the experimental study of HW.

The final and most recent study was conducted by Auguste and Magnaudet (2018) (hereinafter denoted as AM), who systematically explored the parameter space for light rising spheres. The motivation for this numerical study was the discrepancy among the earlier results and the fact that only a single code and numerical method had been employed up till then, though the code versions used by JDB and ZD were not exactly the same (Zhou and Dušek, 2015) and could have been a potential source for the different findings (Auguste and Magnaudet, 2018). Their updated regime map for light spheres is given by Fig. 2. Many new regimes were reported in the intermediate Ga range of 200–300. Most of the results of AM agree fairly well with the numerical results of JDB and ZD and the available experimental results of VB and VBL, while they greatly disagree with the findings of HW; why the results of HW are so different thus remains a puzzling issue. A striking difference with respect to ZD is the extent of the zigzagging regime, which in ZD is limited to $\overline{\rho} \lesssim 0.5$, while it is present up to $\overline{\rho} = 1$ in AM. Furthermore, AM made distinction between a low-frequency zigzagging regime (labelled ZZ) and a high-frequency zigzagging regime for Ga in

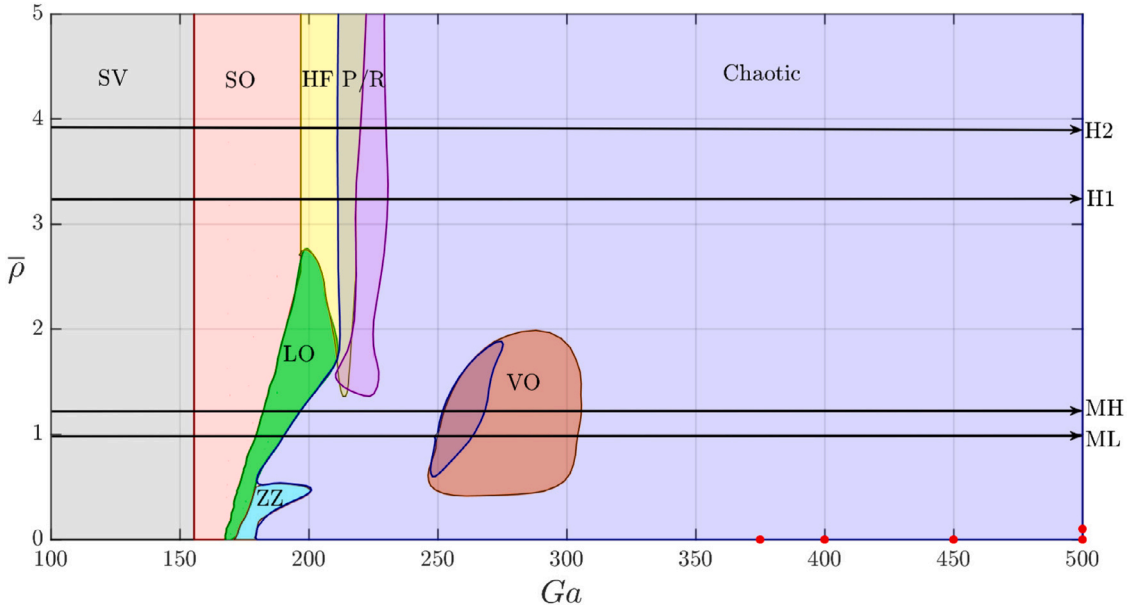

Fig. 1. Regime map by Zhou and Dušek (2015) representing various trajectories of a freely rising/falling sphere. Horizontal black lines represent the region investigated in the present study (explained in detail at the end of Section 1). The annotations are as follows: SV — steady vertical, SO — steady oblique, ZZ — zigzagging, LO — low-frequency oscillating oblique, HF — high-frequency oscillating oblique, P/R — bi-stable chaotic/oscillating oblique regime with fixed planar (P) or slowly rotating (R) symmetry plane, VO — vertical oscillating planar. The red dots correspond to the helical regime. Note that this is a simplified and redrawn version; for the actual version of the regime map we refer to Zhou and Dušek (2015). (For interpretation of the references to colour in this figure legend, the reader is referred to the web version of this article.)

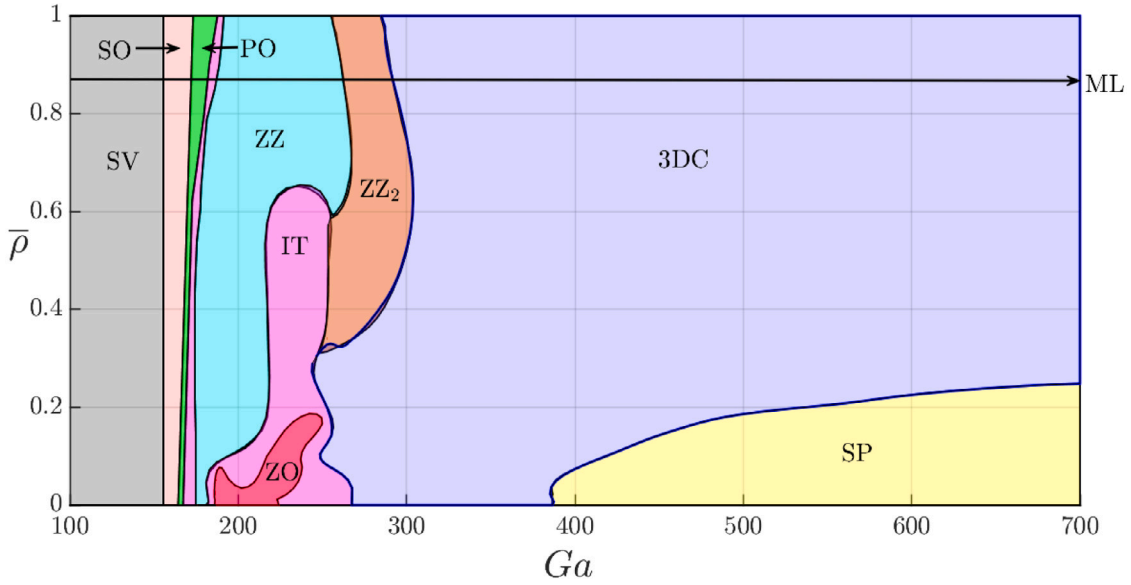

Fig. 2. Regime map by Auguste and Magnaudet (2018) representing various trajectories of a freely rising sphere. The horizontal black line represents the region investigated in the present study (explained in detail at the end of Section 1). The annotations are as follows: SV — steady vertical, SO — steady oblique, PO — periodic oscillating, ZZ — zigzagging, ZZ_2 — zigzag-2, IT — intermittent, ZO — oblique zigzagging, SP — spiralling, 3DC — chaotic. Note that this is a simplified and redrawn version, for the actual version of the regime map we refer to Auguste and Magnaudet (2018).

the range of 250–300 and $\overline{\rho} \gtrsim 0.35$ (labelled ZZ_2). The latter regime is alike the high-frequency vertical oscillating (VO) regime of ZD, but larger in extent on the regime map (cf. Fig. 1 and Fig. 2). Also, no evidence was found of bi-stable behaviour around Ga = 250–260 and $\overline{\rho}$ = 0.5–1 as in ZD. AM also investigated the effect of path instabilities on the drag coefficient. Only for $\overline{\rho} < 0.25$ the drag coefficient was significantly enhanced beyond the C_d for a fixed sphere, with increasing enhancement for lower $\overline{\rho}$. More in particular, for the spiralling regime C_d was found to even increase with increasing Re. This finding is in stark contrast with HW who found the same C_d for all 'vibrating (zigzagging) spheres' ($\overline{\rho} \lesssim 0.3$ for the investigated Re range of AM).

As is clear from the above literature review, the dynamics of path and wake instabilities of a freely rising/falling sphere is far from completely understood. A numerical approach towards exploring various regimes of motion may seem best suited as it allows to cover the entire parameter space in a detailed and systematic manner. But, owing to the complex particle–fluid interactions and the accuracy of the numerical method used, including mesh resolution and domain size, different numerical studies disagree with each other. Also different experimental studies disagree with each other, likely due to the high sensitivity of the particle/wake structure to Ga and $\overline{\rho}$ and the uncertainty in

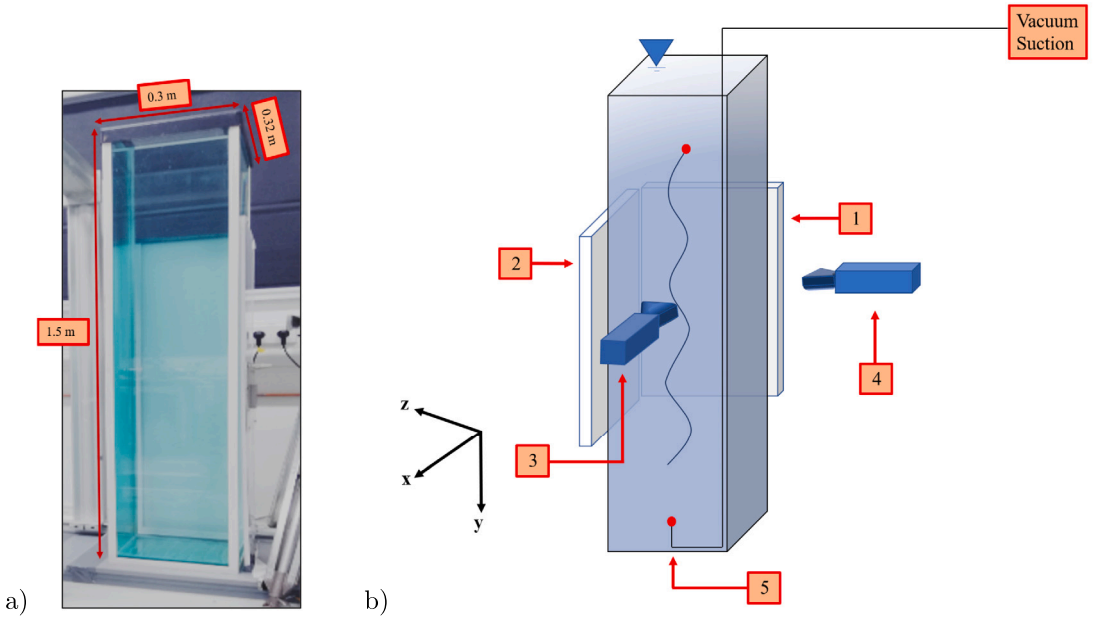

Fig. 3. (a) Settling tank, (b) Schematic showing the LED panels (1,2), cameras (3,4) and the mechanism to release a light sphere from the bottom (5).

determining these numbers accurately. Moreover, improper sphere release and residual disturbances present in the fluid may also affect the particle path. Furthermore, slight inhomogeneities like air voids in the sphere may potentially alter the particle trajectory through a change in the rotational dynamics and the emergence of an additional rotational timescale related to the offset of the centre-of-mass (Jenny et al., 2004; Will and Krug, 2021b). Even in the absence of such an offset, Mathai et al. (2018) highlighted the influence of the moment-of-inertia on the rotational sphere dynamics: hollow spheres with a thin axisymmetric shell, which are often used in experimental studies for investigating the low $\overline{\rho}$ range, may exhibit a different behaviour than homogeneous spheres with the same mass but a correspondingly lower moment-of-inertia (by a factor of approximately 5/3) as considered in numerical simulations. However, recent experiments by Will and Krug (2021a) showed no influence of the moment-of-inertia on the transition between the 3D chaotic and spiralling regime (in both quiescent and turbulent flow) and indicated only a weak effect on the drag coefficient (which increased slightly with decreasing moment-of-inertia in their experiments).

The main aims of the present study are to address the confusions and related disagreements on sphere path instabilities in literature and to characterize the various path instabilities through careful experiments. This requires accurate measurements and a thorough analysis of experimental uncertainties. We have conducted an extensive experimental campaign along with a detailed uncertainty analysis to cover the (Ga, $\overline{\rho}$) parameter space for 219 different combinations of Ga and $\overline{\rho}$, grouped around four values of $\overline{\rho}$ ($\sim$ 0.87, 1.12, 3.19 and 3.9) and Ga in the range of $\sim$ 100 to 700. We will refer to the selected density ratios as 'moderately light' (ML: $\overline{\rho} \sim 0.87$), 'moderately heavy' (MH: $\overline{\rho} \sim 1.12$) and 'heavy' (H1: $\overline{\rho} \sim 3.19$, H2: $\overline{\rho} \sim 3.9$). The choice of the parameters was motivated by our aim to cover as many regimes as possible and especially regimes for which previous studies disagree with each other. For the falling spheres, the regime map of ZD (depicted in Fig. 1) is taken as the prime reference in the discussion of our results as some of their results have already been substantiated experimentally by others. For the rising spheres, the regime maps of both ZD and AM (depicted in Fig. 2) have been taken as the prime references as they have been published recently but appear to disagree with each other for some regimes.

In the experiments we tracked the motion of the sphere in time with two synchronized high-speed cameras using Particle Tracking Velocimetry (PTV) and the corresponding path/regime of motion, velocity statistics and characteristics such as the Strouhal number and drag coefficient have been determined. Comparison is made to the previous studies and the results are also verified for regimes which have been well established earlier.

The outline of this paper is as follows: In the 'Methodology' section, the experimental setup, measurement procedure and data analysis are explained. This is followed by the 'Results' section, where the results are presented for each of the investigated density ratios. Finally, the last section contains a summary and discussion of the main results and the main conclusions.

2. Methodology

2.1. Experimental setup and measurement procedure

The experiments were performed in a glass tank of rectangular cross-section of dimensions $0.30 \times 0.32 \times 1.5$ m^3, see Fig. 3a. The size of the tank was chosen on the basis of the following considerations:

- The sphere is able to travel several hundred sphere diameters (Jenny et al., 2004) before it reaches the field of view of the cameras. This allows the sphere motion and sphere wake to reach a fully developed state.
- It is possible to track the sphere for a sufficiently long distance ($\sim 70d_p$ for the largest sphere in the current study and $\sim 375d_p$ for the smallest one).
- There is negligible effect of side walls in the dynamics of the sphere motion (Di Felice and Parodi, 1996).

Owing to the large volume (144 litres) of the tank, filtered tap water was used for all experiments. The tank was drained and refilled once in 3 to 4 days owing to the increase in the level of contamination over time for still water. The water viscosity was varied by controlling the ambient temperature in the room with air conditioning. In the present study, the water temperature was varied from 16 to 30 ^{o}C. Careful temperature control of the room was crucial as Ga can vary significantly even for 1 degree change in temperature. At the same time, it is important to check for the presence of any temperature gradient along the height of the tank. A PT-100 sensor was used to measure the temperature of water at the top and bottom of the tank. This was done before and after the experiments to confirm the absence of

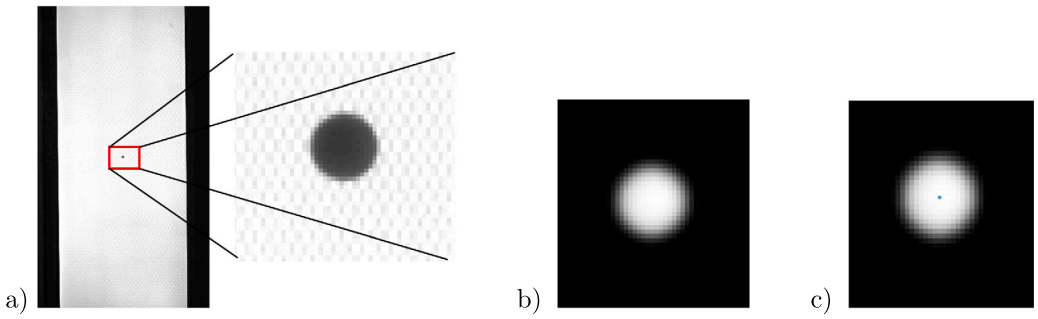

Fig. 4. (a) Raw Image, (b) Image after preprocessing, (c) Estimated centre position.

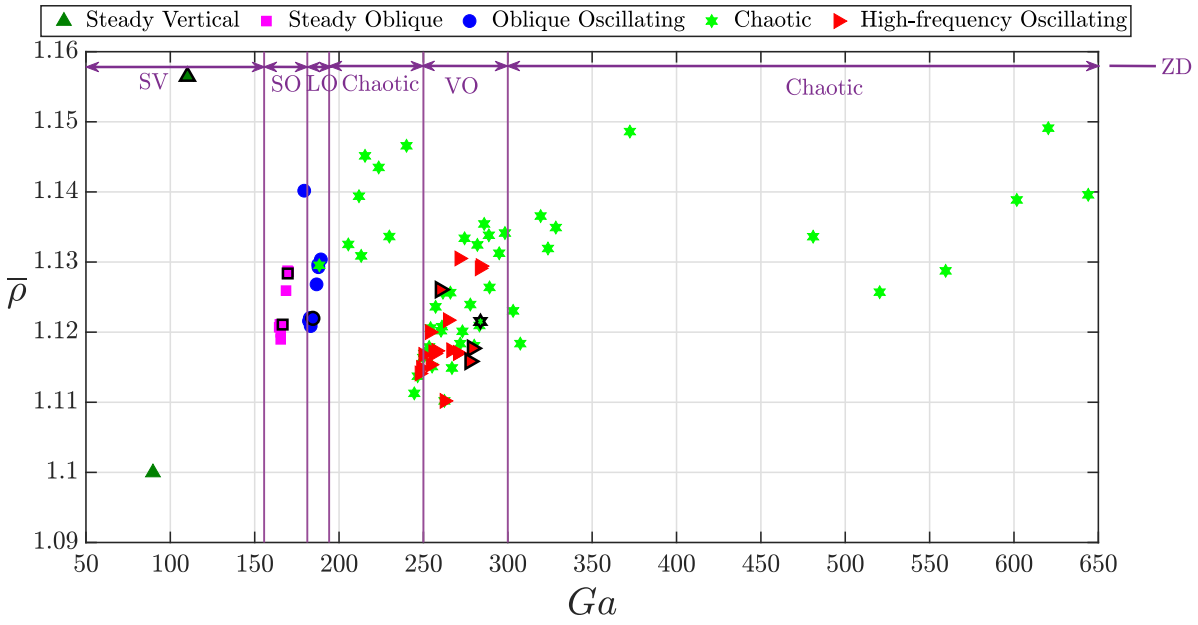

Fig. 5. Regime map updated along line MH with the results of the present study. The markers with a black outline are the cases for which the trajectories are shown. Vertical lines represent the thresholds of different regimes from the ZD map. SV — steady vertical, SO — steady oblique, LO — low-frequency oscillating oblique, VO — vertical oscillating.

any gradients in temperature. Typical temperature differences between the top and bottom of the tank were 0.1–0.2 °C. The uncertainty in the temperature measurement was ± 0.25 °C, which determines the uncertainty in the temperature-dependent water density and kinematic viscosity.

A very vital part of the whole experimental procedure was the quality of the spheres used. As discussed in the introduction section, this can have a significant impact on the regime of motion of the sphere. Precision spheres (with sphericity $\gtrsim 0.99$) of a wide range of diameters with densities ranging from $\sim$ 870 kg/m^3 to 3900 kg/m^3 were purchased from DIT Holland BV, see Table 1. Although a clear disagreement can be seen for lower $\overline{\rho}$ in the maps by ZD and AM, low $\overline{\rho}$ was not considered for the present study. Densities lower than 500 kg/m^3 could not be covered simply due to the unavailability of *homogeneous* solid spheres in such density ranges and, as discussed in the introduction section, hollow spheres exhibit different rotational dynamics than homogeneous solid spheres (Mathai et al., 2018). The motivation for the selected $\overline{\rho}$ was already given in Section 1. We remark that all selected $\overline{\rho}$ are of $O(1)$ and also $\gg 1/\sqrt{Ga}$. According to the classification of AM, they fall in the *intermediate* to *dense* regime in which the viscous Stokes boundary layer has negligible influence on the translational and rotational sphere dynamics and the influence of added mass on the translational sphere dynamics is progressively reduced for increasing density ratio (weaker fluid/solid coupling).

The properties of the spheres used in the present study are listed in Table 1. For each individual sphere, the density was precisely determined by measuring its mass and diameter. The mass was measured using a weighing scale with an uncertainty of 0.07 mg. The diameter was measured using a microscope with an uncertainty of $\sim$ 20 μm (see supplementary material). Despite careful selection of the spheres, for the polypropylene and nylon spheres the presence of small air voids inside the sphere cannot be excluded since these spheres were manufactured using injection moulding. Histograms of the density of the spheres are shown in Figs. 26 and 27 in Appendix A. For the polypropylene spheres, the standard deviation of the distribution is $\simeq$ 2% of the mean value. This is still of the same order as the ~2% measurement uncertainty (see Fig. 30 in Appendix B). Also, we refrained from using polypropylene spheres with outlier values for the mass density (with the exception of 1 case around $Ga = 120$ in the steady, *non-rotating*, vertical regime, see Fig. 30). Thus, we deem the effect of air voids on the moment-of-inertia and on the offset in the centre-of-mass from the geometrical centre small, although we are not able to quantify this more precisely. The same argument holds for the nylon spheres, with a standard deviation of the distribution of $\simeq$ 0.9% of the mean value. For the silicon nitride and aluminium oxide spheres, the standard deviation of the distribution is $\simeq$ 0.9 and $\simeq$ 1.4%, respectively, which is significantly smaller than the measurement uncertainty of ~2.5% for the lower Ga range, see Fig. 29.

For the spheres heavier than water, a tweezer is used to release the sphere from the top of the tank. Using a tweezer as a release tool was

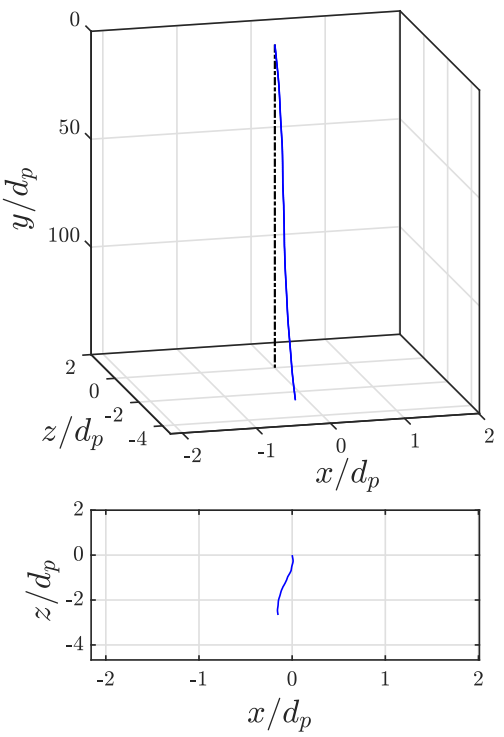

Fig. 6. Steady vertical trajectory with slight drift for $\bar{\rho}$ = 1.156 and Ga = 110.14, falling with a mean vertical velocity ($\overline{v}_y/v_g$) of 1.01.

Table 1
Sphere specifications provided by the supplier (note that measured values for each and every particle slightly deviate from the approximate values given here).

Material	Type	Density (ρ_p) (kg/m^3)	Diameter (d_p) (mm)
Polypropylene	Plastic	~ 870	~ 2, 3.5, 4
Nylon	Plastic	~ 1120	~ 2, 3, 4, 4.5, 5.56, 6.35
Silicon Nitride	Ceramic	~ 3190	~ 1.2, 2.38
Aluminium Oxide	Ceramic	~ 3900	~ 1.2, 2, 2.38

recently reported by Toupoint et al. (2019). The sphere is pre-wetted (to avoid the possibility of air bubbles being created when released) and is held by the tweezer. It is gently taken below the free surface of the tank and released manually after some time to allow the perturbations to vanish first. Although we cannot exclude that the tweezer might still have had a small effect on the initial sphere motion, we have not observed it to trigger any aberrant behaviour on the final path taken by the sphere. Furthermore, tests with different release mechanisms such as a robotic gripper arm and vacuum suction gave consistent results, see Raaghav (2019) for details. The tweezer was finally chosen because of the simplicity of use.

For spheres lighter than water, a vacuum pump was used to release the sphere from the bottom of the tank. This is shown in Fig. 3b. The sphere is taken to the bottom of the tank and is held at rest at the bottom for at least two hours by connecting it via a tubing network to a vacuum pump. After that, the vacuum pump is switched off and the sphere is allowed to rise gently. A discussion regarding the design and details of the release mechanism can be found in Raaghav (2019).

2.2. Particle tracking and signal processing

The goal of the present study is to track the 3D motion of a single rising or falling sphere and to capture various path instabilities accurately. A pair of synchronized cameras was used to image and track the motion of the sphere. Based on the availability, either a pair of Imager sCMOS (LaVision; 2560 × 2160 pixels, 16 bit) or a pair of Imager Pro HS (LaVision; 2000 × 2000 pixels, 12 bit) cameras was used. The cameras were equipped with a Nikon AS-S DX 35 mm objective. The f-number of the objectives was set to 16 in order to have a large depth of field covering most of the tank. The frame rate of the cameras ranged from 50 to 500 Hz depending upon the case investigated. Both cameras had a field of view of 45 cm in the vertical direction, which provides adequate distance to track the sphere in time. Depending upon the camera used, the resolution was 0.208 mm/pixel for Imager sCMOS and 0.223 mm/pixel for Imager Pro HS. Two LED panels were used for backlighting, so that the moving sphere appears as a dark circle on the bright illuminated background. The schematic of the camera and LED setup is depicted in Fig. 3b.

Proper calibration of the cameras is essential to account for the change in refractive indices across interfaces (air, glass and water) and to correct from various other distortions. An in-situ calibration procedure following Soloff and Adrian (1997) was used in the present study. The RMS error of the calibration ranges from 0.4 to 0.89 pixels, corresponding to approximately 0.09 mm to 0.2 mm (Raaghav, 2019). We take the upper limit (0.2 mm) as a conservative estimate of the uncertainty in position.

3D particle tracking velocimetry is used to study the motion of the sphere in time. The particle tracking algorithm was implemented in MATLAB following the approach of Maas et al. (1993) and Nicholas et al. (2006).

The postprocessing of the acquired images can be summarized as follows:

1. The pair of images of the two cameras is imported. These are the raw images and an example of a raw image is depicted in Fig. 4a.
2. From each of the raw images the background image is subtracted, which is the image taken before the particle is released. This removes any form of unwanted spurious information in the image, thereby leaving us with a bright circle (particle) on a dark background. Following this, a band pass filtering is applied using the MATLAB routine *bandpass.m* (Daniel and Dufresne, 2008) to further smooth out the bright spot (Fig. 4b).
3. To estimate the centre of the bright circle, firstly, the pixel position corresponding to the highest intensity is detected. Then a search window is defined around this high intensity pixel. Using the (x, y) values and the intensity values $I(x, y)$ of the pixels within this search window, a weighted centroid averaging method (Nicholas et al., 2006) is implemented to compute the centre of the particle (Fig. 4c). The corresponding equation is as follows:
$$(x_c, y_c) = \left(\frac{\sum_{n=1}^{N} x_n I(x_n, y_n)}{\sum_{n=1}^{N} I(x_n, y_n)}, \frac{\sum_{n=1}^{N} y_n I(x_n, y_n)}{\sum_{n=1}^{N} I(x_n, y_n)} \right). \quad (2)$$
Here (x_c, y_c) is the coordinate of the particle centre, n stands for the index of the pixel within the search window considered and N is total number of cells within the window. (x_n, y_n) is the coordinate of each pixel with intensity $I(x_n, y_n)$. Thus, at the end of this step, we obtain two coordinates, $(x_c, y_c)_{camera_1}$ and $(x_c, y_c)_{camera_2}$.
4. With the particle centres computed from both the images, the centre coordinate in each image is mapped onto the two calibration planes using the polynomials obtained from calibration. Thus, we will have four (X, Y) coordinates, namely, $(X, Y)_{c_1,p_1}$, $(X, Y)_{c_1,p_2}$, $(X, Y)_{c_2,p_1}$ and $(X, Y)_{c_2,p_2}$, where the subscripts c and p correspond to camera and calibration plane, respectively.
5. Triangulation is performed using the four coordinates to reconstruct the 3D coordinate (Hartley and Zisserman, 2003).
6. The above steps are repeated for all image pairs acquired from the experiment.

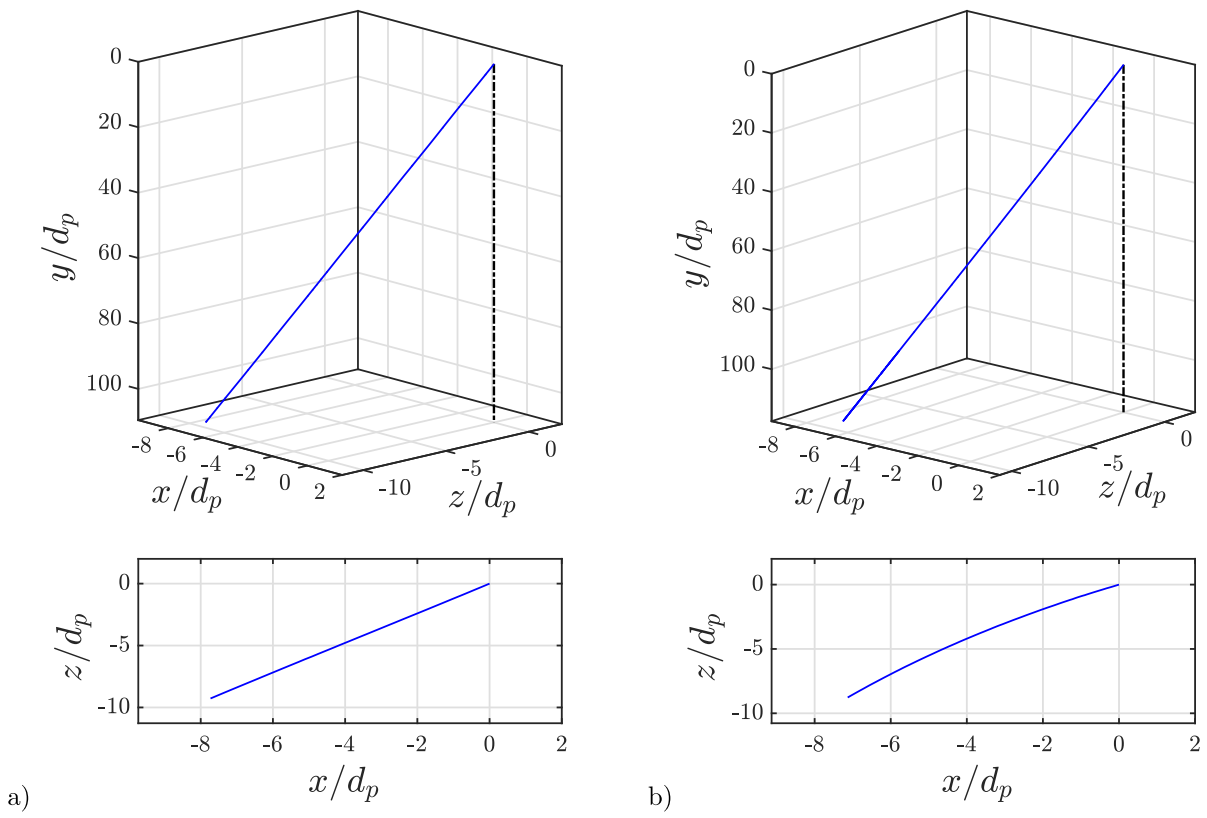

Fig. 7. (a) Steady oblique trajectory for $\overline{\rho}$ = 1.121 and Ga = 166.56 falling at an angle of 6.28° with respect to the vertical, with a mean vertical velocity ($\overline{v}_y/v_g$) of 1.46 and mean horizontal velocity ($\overline{v}_h/v_g$) of 0.16, (b) Curved steady oblique trajectory for $\overline{\rho}$ = 1.128 and Ga = 169.57 falling at an angle of 5.24° with respect to the vertical, with a mean vertical velocity ($\overline{v}_y/v_g$) of 1.37 and mean horizontal velocity ($\overline{v}_h/v_g$) of 0.13.

The position coordinates obtained from the particle tracking routine often have noise associated to them due to the finite pixel size and image noise. Therefore, in the present study, a Savitzky–Golay filter (Savitzky and Golay, 1964) is employed, which is a moving polynomial filter. For a given frame length (set of points), a polynomial of order 3 is fit through the points. This polynomial can then be analytically differentiated to compute higher-order statistics like velocity and acceleration. The optimal frame length is determined from the requirement to suppress spurious noise as much as possible but to preserve the physical signal of interest at the same time. To this purpose we computed the standard deviation of the velocity signal obtained from a filtered trajectory as function of the chosen frame length. Typically, the standard deviation first quickly drops with increasing frame length (associated with the high-frequency noise that is removed), then it varies only weakly with frame length over a large interval, and finally it starts decreasing again at large frame lengths (associated with the physical signal that is now filtered out). The optimal frame length was set to the mid value of the intermediate interval. The optimal value was determined for each camera frame rate and the different sphere materials used (as the frequency of path instabilities depends on the particle/fluid mass density ratio and hence on the particle mass density). Also, when computing the spectrum of the velocity signal, we applied detrending and a Hanning window to avoid spectral leakage. Detailed documentation regarding signal processing performed in the present study can be found in Raaghav (2019).

3. Results

All the plots presented in this section are non-dimensionalized as follows. Position is normalized with the sphere diameter (d_p). The horizontal velocities (v_x and v_z), vertical velocity (v_y) and the absolute horizontal velocity ($v_h = \sqrt{v_x^2 + v_z^2}$) of the sphere are normalized with the inertio-gravitational velocity (v_g). The frequency is either normalized by the gravitational frequency ($\overline{f} = f/f_g$ with $f_g = \sqrt{\frac{|\overline{\rho}-1|g}{d_p}}$) or by the mean vertical velocity and particle diameter to obtain the Strouhal number ($St = f\, d_p/|\overline{v}_y|$). Whenever it is mentioned 'moving along line MH/H1/H2/ML' in the sequel, it means that Ga is increased at a fixed $\overline{\rho}$.

3.1. Falling sphere — moderately heavy case ($\overline{\rho} \sim 1.12$)

In Fig. 5 the regime map obtained in the present study when moving along line MH is shown. The markers represent the results of the present measurement campaign and the vertical lines are regime borders from ZD at $\overline{\rho} \sim 1.12$. For the moderately heavy case, nylon spheres were used and a total of 87 different measurements were performed. Each marker corresponds to a separate release. The measurements include that of different spheres and also multiple measurements with the same sphere at different water temperatures.

It is important to note that, when the same sphere was released again, the density was remeasured because of the possible slight change in mass of the sphere due to water absorption during the previous experiment. Evidence of water absorption was found only for the nylon spheres. Tests with prolonged immersion of a nylon sphere in water showed an increase in the sphere mass of 0.7% and 1.3% after, respectively, 2 and 5 h. Thus the effect of water absorption during a fall experiment itself is negligible as an experiment took typically only a few minutes (from pre-wetting to release and settling at the bottom of the tank). However, released spheres were collected from the bottom of the tank only after the end of an experimental campaign (typically after 1–2 h), and hence we dried them in an oven at 40 °C before reusing them. More details on the effect of water absorption by submerged nylon spheres can be found in Raaghav (2019). Finally, we note that

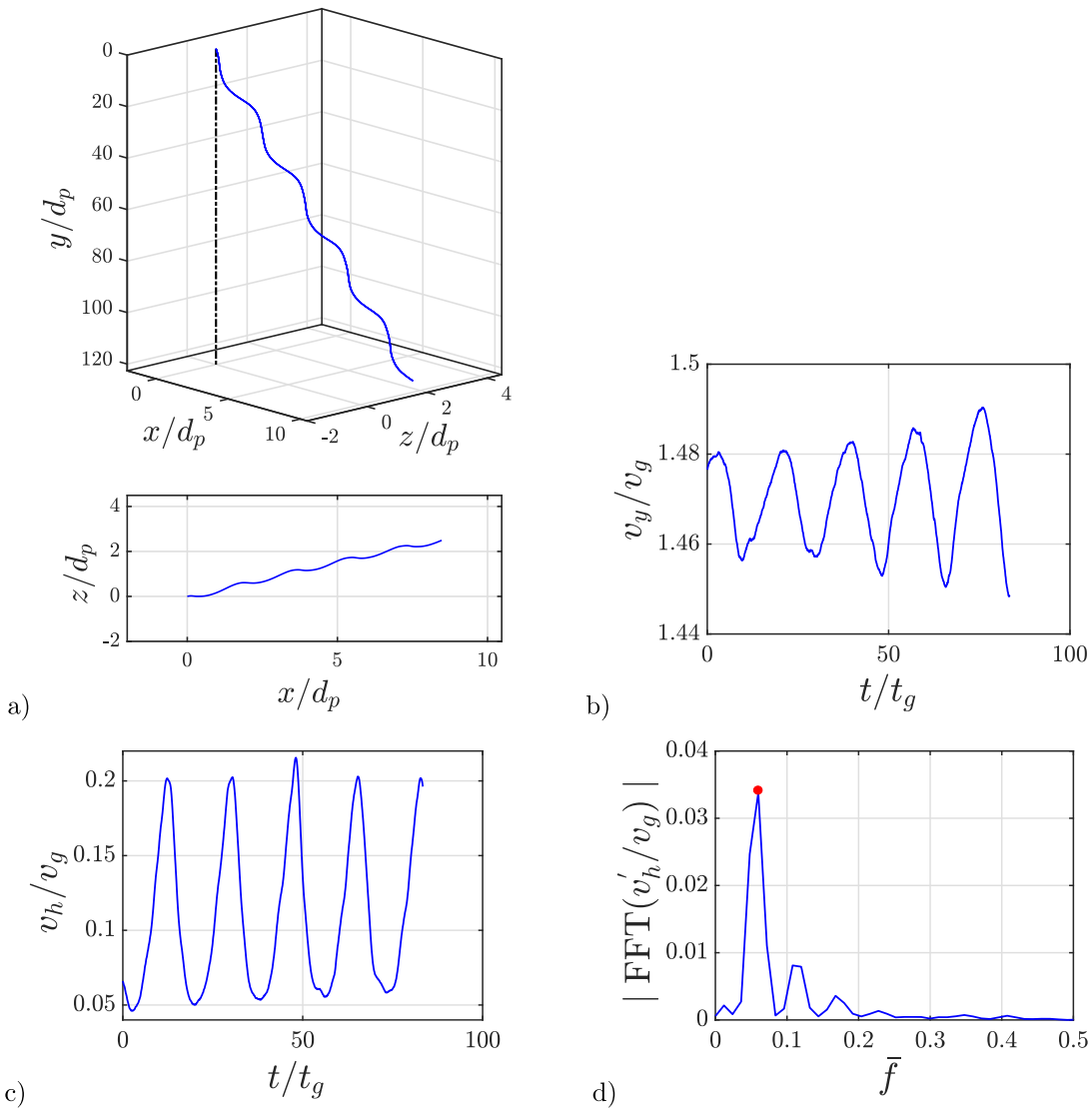

Fig. 8. (a) Oscillating oblique trajectory for $\bar{\rho}$ = 1.121 and Ga = 184.46 and with an average angle of 3.74° with respect to the vertical, a mean vertical velocity ($\overline{v}_y/v_g$) of 1.47 and a mean horizontal velocity ($\overline{v}_h/v_g$) of 0.11, (b) Temporal variation of vertical velocity (amplitude of oscillation $\sim 0.013v_g$), (c) Temporal variation of horizontal velocity (amplitude of oscillation $\sim 0.075v_g$), (d) Spectrum of the fluctuation of horizontal velocity (with the red dot indicating the dominant peak at 0.059). (For interpretation of the references to colour in this figure legend, the reader is referred to the web version of this article.)

the same regime map as Fig. 5 but with the experimental uncertainty included for every data point, is provided in Appendix B. This indicates that the scatter in density ratio in Fig. 5 falls within the experimental uncertainty.

Steady vertical regime

For Ga < 155 both the falling and rising spheres will have an axisymmetric wake and will fall/rise in a steady vertical path. The older map by JDB and the updated version by ZD report the above threshold without any disagreement. Moreover, this was also observed experimentally by HW. The focus of the current study, will be on the non-vertical regimes for Ga > 155. It is important to note that a perfect vertical path is very difficult to achieve in experiments. The sphere will always have a small drift that makes the path deviate from the strictly vertical trajectories found in numerical studies. This drift is random and not reproducible. It is caused by the presence of residual disturbances in the fluid which are very difficult to avoid in practical conditions. Moreover, the sphere is never a perfect/ideal sphere like the ones employed in numerical simulations. A similar argument is also mentioned by Ellingsen and Risso (2001), Fernandes et al. (2007) and Toupoint et al. (2019) for bubbles and discs. A typical trajectory in the steady vertical regime with a slight drift is shown in Fig. 6. The horizontal drift is about 2.2% of the total vertical distance travelled by the sphere. This corresponds to an average angle of ~ 1.3° with respect to the vertical in this case, which is much smaller than the falling angles found for the steady oblique regime at higher Ga discussed next. There are possible ways to correct for the drift (Ellingsen and Risso, 2001), which is, however, beyond the scope of the present study.

Steady oblique regime

For Ga > 155 JDB report the breaking of the axisymmetric wake and transition to a planar symmetric wake with a slight inclination angle of the plane of symmetry with respect to the vertical. The orientation of the symmetry plane is random in the azimuthal direction (set by the initial perturbation that triggers transition) and results in what is referred here as a **'steady oblique'** regime. It is clear from the present map (Fig. 5) that the steady oblique regime was also observed in the present study in the same Ga range. A typical oblique motion of a sphere obtained from our experiments is depicted in Fig. 7a. This regime was also observed experimentally by VB and HW. Not many data points were considered within this regime in the present study as the characteristics of this regime have already been established in

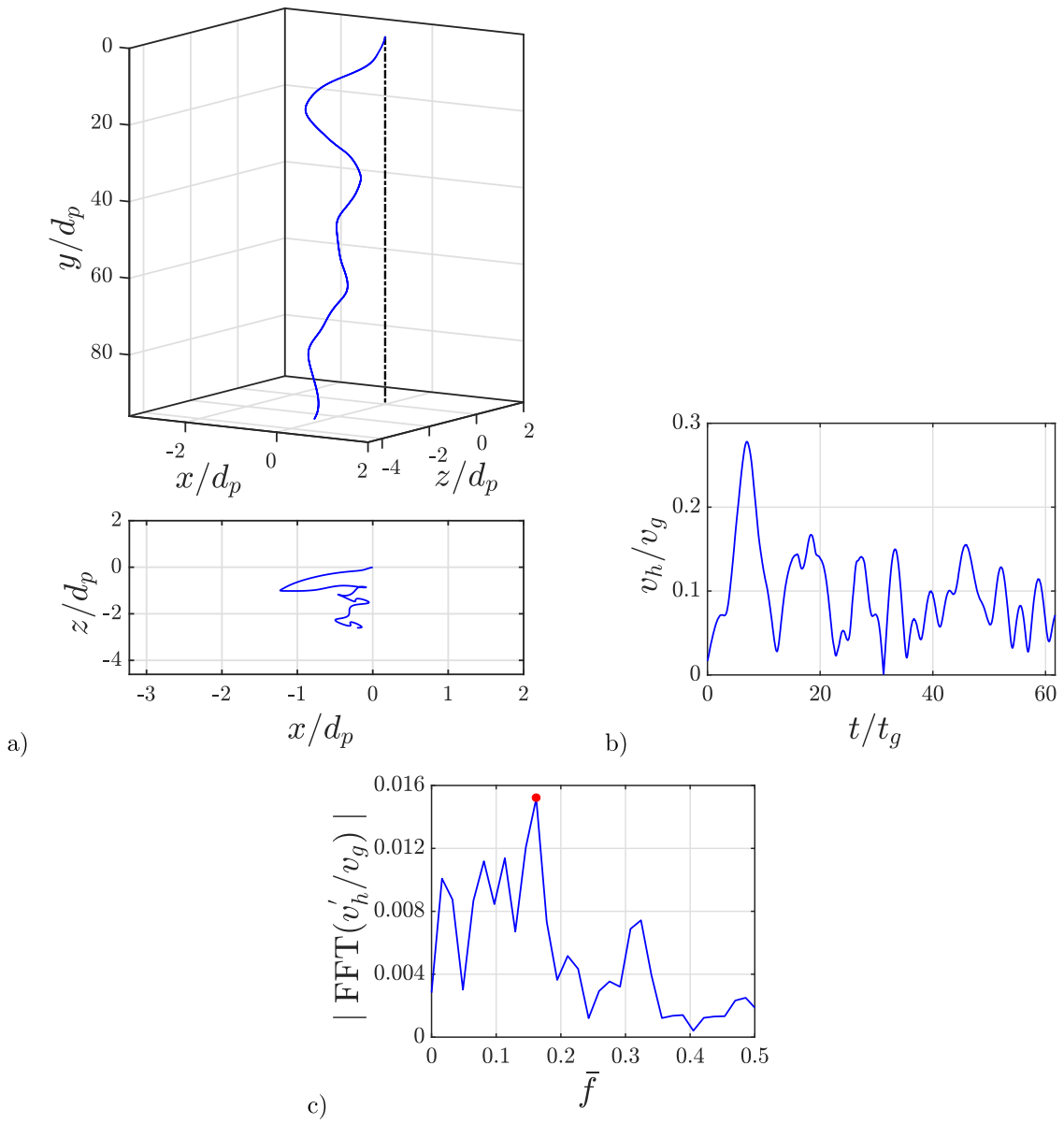

Fig. 9. (a) Chaotic trajectory for $\bar{\rho}$ = 1.121 and Ga = 283.81, (b) Temporal variation of horizontal velocity, (c) Spectrum of the fluctuation of horizontal velocity (with the red dot indicating the dominant peak at 0.161). (For interpretation of the references to colour in this figure legend, the reader is referred to the web version of this article.)

great detail. The primary goal here was to verify that our experimental methodology can reproduce this regime. For the cases investigated, the angle with respect to the vertical agrees with the earlier studies. For the steady oblique regime, this angle was simply determined from the first and the last measured position, as the path was generally found to be rectilinear in this regime. For cases in which the sphere oscillates, as in the oscillating oblique regime discussed next, we computed the mean angle from the average over the local angle (obtained from the dot product of the vertical unit vector with the local tangent unit vector along the sphere trajectory). Table 2 shows the comparison of the angles obtained in other studies and the values from the present study. The table collectively represents the range in angle for both the steady oblique regime and the oscillating oblique regime. We remark that a few of the results in the present study show a curved oblique path (Fig. 7b) and some small angles found in the present are related to this. Similar curved trajectories were also observed by VB in their experiments, which they attributed to a slight deviation of the particle's shape from a perfect sphere and/or an inhomogeneous mass distribution within the sphere.

Table 2
Presently found and previously reported angles with respect to vertical for the steady and oscillating oblique regimes of the moderately heavy and moderately light spheres.

Research article	Angle (°)
Present study	~ 2.8 to 7.4
HW (see their Fig. 22)	~ 4 to 7.5
ZD (see their article page 207)	~ 4 to 6
AM (see their article page 237,238)	~ 4.3 to 4.5

Oscillating oblique regime

Moving along Line MH in Fig. 1, beyond a critical Ga, the planar wake undergoes a Hopf bifurcation and the oblique trajectory of the sphere begins to oscillate, leading to a new regime known as the **'oscillating oblique'** regime. The transition from the steady oblique to the oscillating oblique regime can be clearly seen in Fig. 5. A trajectory in this regime is depicted in Fig. 8a and the corresponding

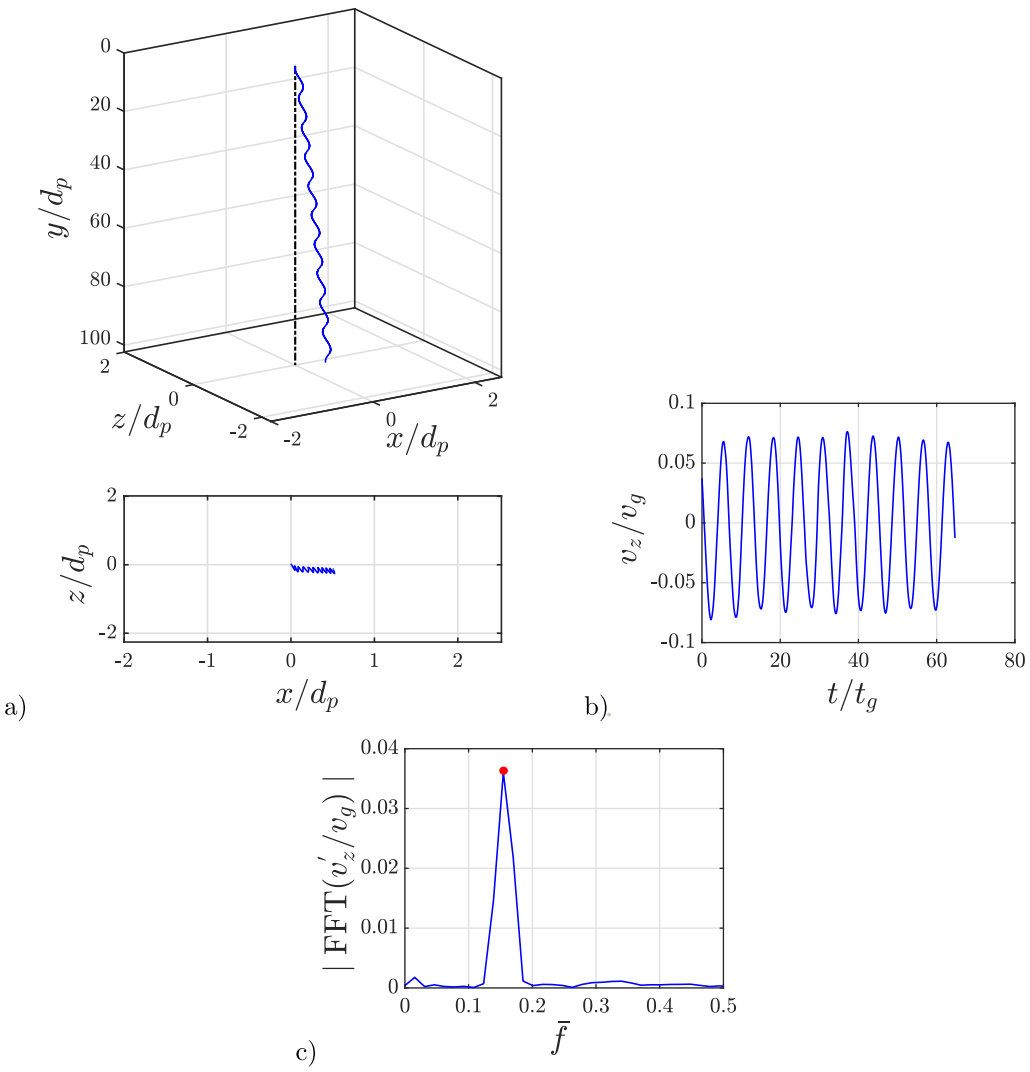

Fig. 10. (a) High-frequency oscillating trajectory for $\overline{\rho}$ = 1.126 and Ga = 259.92, (b) Temporal variation of velocity in z-direction, (c) Spectrum of the fluctuation of velocity in z-direction (with the red dot indicating the dominant peak at 0.154). (For interpretation of the references to colour in this figure legend, the reader is referred to the web version of this article.)

time evolution of the vertical and the horizontal velocity is shown in Fig. 8b,c with the amplitudes of the velocity oscillation being $\sim 0.013v_g$ and $0.075v_g$, respectively. The trend in oscillation amplitude in Fig. 8b is not a common feature for all cases in the oscillating oblique regime, but is occasionally present (in another case the amplitude is actually decreasing); it is unclear where the increasing trend originated from in this particular case. Similar to the steady oblique cases, a curved oscillating path was also observed in a few cases.

The critical Ga for the onset of this regime corresponds to $Re \sim 240$, which is well below the critical Re for the onset of shedding for a fixed sphere of $\sim$ 275 (Ghidersa and Dušek, 2000). This clearly indicates that the effect of additional degrees of freedom of a freely settling sphere is evident from the quicker transition behaviour, as noted by AM. The frequency of shedding is computed from the dominant peak in the frequency spectrum (Fig. 8d). As mentioned earlier, we employ a Hanning window over the velocity signal. In order to do this, first, we correct for linear trends in the velocity signal by subtracting a linear fit. Hence we work with the remaining velocity deviations signal (v_h'). Subsequently, a Hanning window is applied to v_h' and finally the spectrum is computed; more details can be found in Raaghav (2019). We can clearly see a peak at $\overline{f}$ = 0.059. This $\overline{f}$ is much smaller than the frequency of the corresponding secondary (Hopf) bifurcation found for a fixed sphere, and originates from the strong fluid/solid interaction at low density ratio (referred to as a solid-mode interaction by ZD). This is the reason why this regime is also called 'low-frequency oscillating oblique' regime by ZD. For the low-frequency oscillating oblique regime observed in the present study, $\overline{f}$ is in the range of 0.046 to 0.059, which agrees very well with the previously reported range of 0.045 to 0.068 by JDB and 0.064 to 0.076 by ZD. So there is no disagreement between the present study and previous studies for the steady vertical, steady oblique and oscillating oblique regimes. This serves as a good validation of the present methodology.

Chaotic regime and hidden bi-stable regime

Moving along Line MH in Fig. 1, at $Ga \sim 200$ ZD observed a transition to chaos. From the present results, we agree with ZD as a **'chaotic regime'** is also observed for various Ga considered from 205 to 243 (depicted in Fig. 5). In the present study, the chaotic regime was observed up to the highest Ga employed. One such case in the chaotic regime is depicted in Fig. 9. The path taken in the chaotic regime is not repeatable, but contains intermittent imprints of the stable regimes for nearby Ga values in the (Ga, $\overline{\rho}$) parameter space. This is clear from the spectrum of the chaotic regime (Fig. 9c), where we see a dominant peak at $\overline{f}$ = 0.161 and also a few low frequency peaks close to it. This was also unequivocally observed from numerical simulations by JDB, ZD and from the experiments of VB. Furthermore, this observation matches with the spectrum for fixed spheres where $\overline{f}$ of 0.045 and 0.167 was

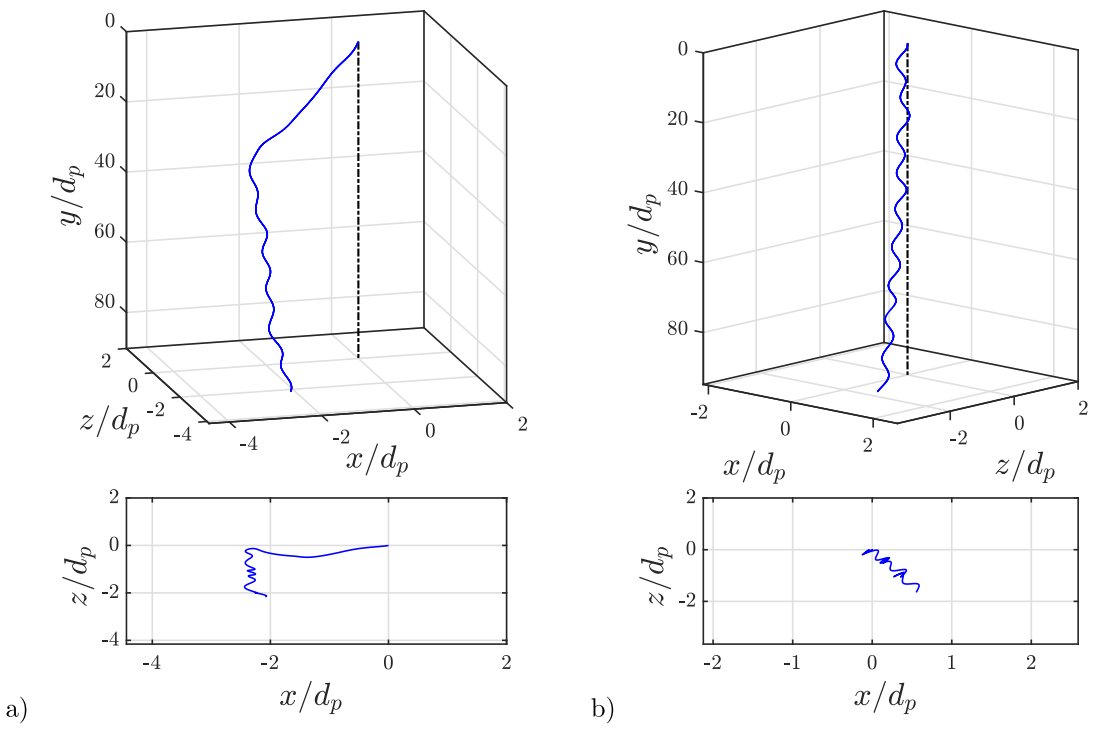

Fig. 11. (a) Transition from a drifting chaotic trajectory to a high-frequency oscillating trajectory at $\overline{\rho}$ = 1.117 and Ga = 278.95, (b) Irregular high-frequency oscillating trajectory at $\overline{\rho}$ = 1.115 and Ga = 277.49.

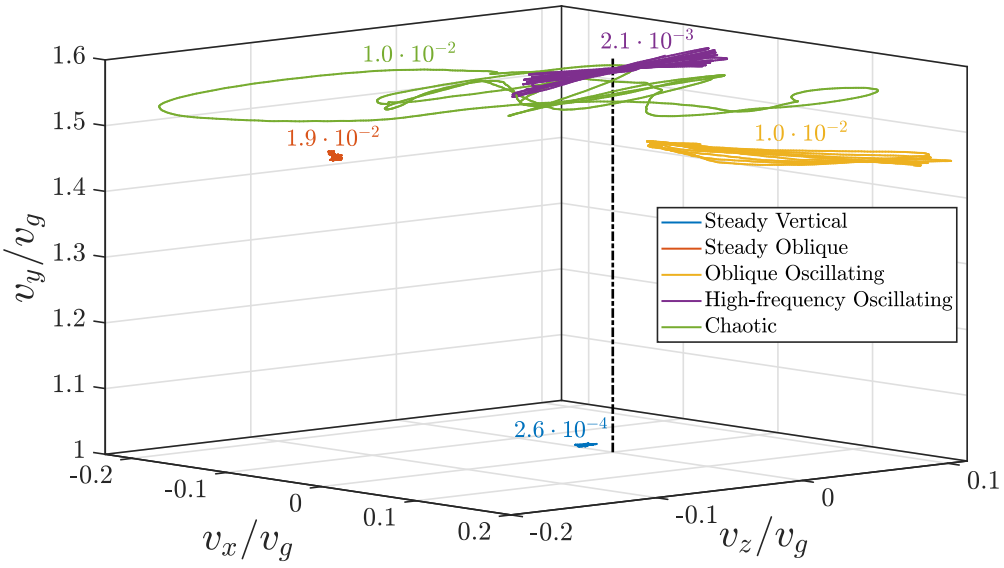

Fig. 12. 3D velocity plot for all the regimes along line MH, with Ga and $\overline{\rho}$ for each regime corresponding to: Steady Vertical — Ga = 110.14 and $\overline{\rho}$ = 1.156, Steady Oblique — Ga = 166.56 and $\overline{\rho}$ = 1.121, Oscillating Oblique — Ga = 184.4 and $\overline{\rho}$ = 1.121, High-frequency oscillating — Ga = 259.92 and $\overline{\rho}$ = 1.126, Chaotic — Ga = 283.81 and $\overline{\rho}$ = 1.121. The numbers in the plot are the values of η (see Eq. (3c)) for each regime.

observed at Re = 500 (Tomboulides and Orszag, 2000). The presence of this dominant frequency also hints at the possible existence of a high-frequency oscillating regime for nearby Ga values with $\overline{f} \approx 0.16$. This brings us to the discussion of the next regime.

Moving along Line MH in Fig. 1, for $Ga \sim 250$ to 300 ZD report a strictly vertical regime (2D) with high-frequency oscillations, called the **'vertical oscillating'** regime. For $\overline{\rho}$ slightly greater than 1, ZD had probed four points in this Ga interval and two of them were characterized as stable vertical oscillating cases and the other two as bi-stable in which the sphere is either falling in the chaotic (intermittent) regime or in the vertical oscillating regime dependent of the initial condition. This was not reported in the older study by JDB, but a similar bi-stable regime was reported by them for *rising* spheres ($\overline{\rho} < 1$). However, in their updated map (Fig. 1), this zone is very clearly present and a distinction between bi-stable and fully stable regimes is made. Owing to this disagreement and also owing to the fact that this regime was not studied experimentally before, we decided to probe this regime in detail. Almost 45 different Ga values were investigated ranging from 250 to 300 and a clear cloud of the above vertical oscillating mode was observed, see Fig. 5.

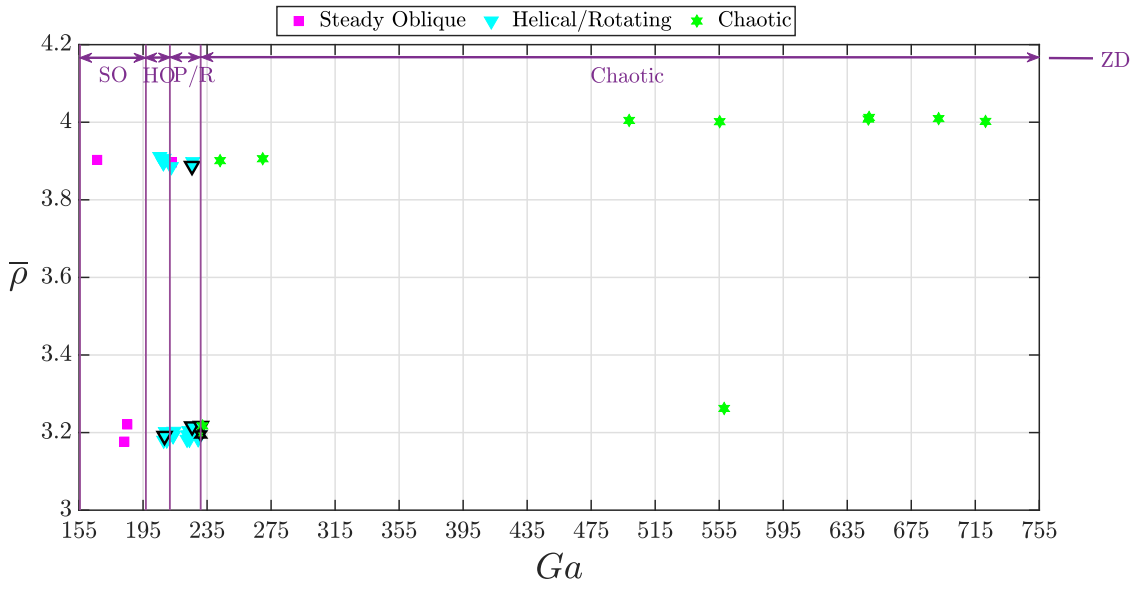

Fig. 13. Regime map updated along lines H1 and H2 with the results of the present study. The markers with a black outline are the cases for which the trajectories are shown. Vertical lines represent the thresholds of different regimes from the ZD map. SO — steady oblique, HO — high-frequency oscillating oblique, P/R — planar/rotating or chaotic bi-stable regime.

As mentioned earlier, pure vertical trajectories are very difficult to obtain experimentally. A slight drift was typically present, making it deviate from the strictly vertical nature mentioned by ZD. Due to the small drift, the above regime will here be referred to as a **'high-frequency oscillating'** regime although the characteristics are similar to the vertical oscillating regime mentioned by ZD. A typical trajectory of the high-frequency oscillating regime is depicted in Fig. 10a along with the temporal evolution of horizontal velocities and the corresponding spectra in Fig. 10b,c. A clear peak is seen at $\overline{f} = 0.154$. It is interesting to note that a similar range of $\overline{f}$ has been observed during vortex shedding past a fixed sphere at $Re = 500$ (Tomboulides and Orszag, 2000). In the present study, this regime was not observed to be the only stable asymptotic state, but it is coexisting with a chaotic regime. Out of the 45 different measurement points in the $(Ga, \overline{\rho})$ map, close to 26 were observed to be in the chaotic regime and 19 were observed to be high-frequency oscillating (indicated by different symbols in Fig. 5). In some cases, a smooth transition from chaos to the high-frequency oscillating regime was seen (Fig. 11a), while in some other cases clear irregular unstable high-frequency oscillations were observed (Fig. 11b). This is indicative of a bi-stable nature. At this point we would like to make two remarks. First, there is a possibility that after a much longer distance of travel by the sphere, only one regime may exist, making it purely chaotic or purely high-frequency oscillating. Second, since we observe from Fig. 5 that the high-frequency and chaotic regimes are both spread out over the entire range of Ga from $\sim$ 240 to 280, we qualify this regime as bi-stable. ZD reported that for $Ga \sim 250$ to 300 the trajectories fall within a fully stable vertical oscillating regime, so our results disagree with this. For $Ga > 300$, we consistently observed a chaotic regime, which is in agreement with ZD again.

Similar to AM, we plotted the three velocity components (v_x, v_y and v_z) in Fig. 12 for all the regimes observed when moving along line MH. This aids to better understanding of the transition to chaos. It is clear from the velocity diagram that with an increase in Ga the area occupied in the 3D space increases. The steady vertical regime appears almost as a dot (owing to negligible horizontal excursions), while the chaotic regime exhibits the greatest velocity excursions. From the steady oblique regime to the chaotic regime, the magnitude of the horizontal velocity fluctuations increases, indicating that the solid–fluid coupling is becoming stronger. For a more quantitative picture, we estimated the fraction of work by gravity that is lost to drag acting on horizontal sphere motions (η). On statistical average, the work by the net gravity force on the particle motion is equal to:

$$\overline{W}_g = \left|\rho_p - \rho_f\right| \frac{1}{6}\pi d_p^3 g \left|\overline{v}_y\right| = \frac{1}{6}\pi d_p^2 \rho_f v_g^2 \left|\overline{v}_y\right|. \tag{3a}$$

Similarly, the work by the "steady" drag force acting in the horizontal direction, can be written as (Magnaudet, 1997, based on his Eq. (3) for the drag force):

$$\overline{W}_{dh} = -C_d \frac{1}{8}\pi d_p^2 \rho_f \overline{\sqrt{v_h^2 + v_y^2} \cdot v_h^2}, \tag{3b}$$

where C_d is assumed to be constant (basically by assuming that $C_d \approx C_d(|\overline{v}_y| d_p/\nu_f)$). Assuming further a drag coefficient $C_d = O(1)$, the fraction (η) of work by gravity that is lost to drag acting on the horizontal sphere motions, is then equal to:

$$\eta = -\frac{\overline{W}_{dh}}{\overline{W}_g} = \frac{3}{4} \frac{\overline{\sqrt{v_h^2 + v_y^2} \cdot v_h^2}}{v_g^2 \left|\overline{v}_y\right|}. \tag{3c}$$

Typical values of η are shown in Fig. 12 for the different trajectories. The highest value of η is found for the steady oblique regime ($1.9 \cdot 10^{-2}$) followed by the oscillating oblique and chaotic regimes ($1.0 \cdot 10^{-2}$), while it is lowest for the steady vertical regime ($2.6 \cdot 10^{-4}$), which suggests that the drag coefficient (C_d) for the oblique and chaotic modes will likely be most affected as compared to the fixed-sphere counterpart. Note, however, that in all cases the value of η is still small, suggesting already that the effect of path instabilities on C_d is small too.

3.2. Falling sphere — heavy cases ($\overline{\rho} \sim 3.19$ and 3.9)

In Fig. 13 the regime map obtained when moving along lines H1 and H2 is shown. The markers represent the results of the present measurement campaign and the vertical lines are adapted from ZD and show the thresholds between different regimes. The same map with the uncertainties included for every case is provided in Appendix B. For the high density cases, 7 Silicon Nitride spheres and 11 Aluminium Oxide spheres were used and a total of 44 different measurements were performed. The measurements included that of different spheres and

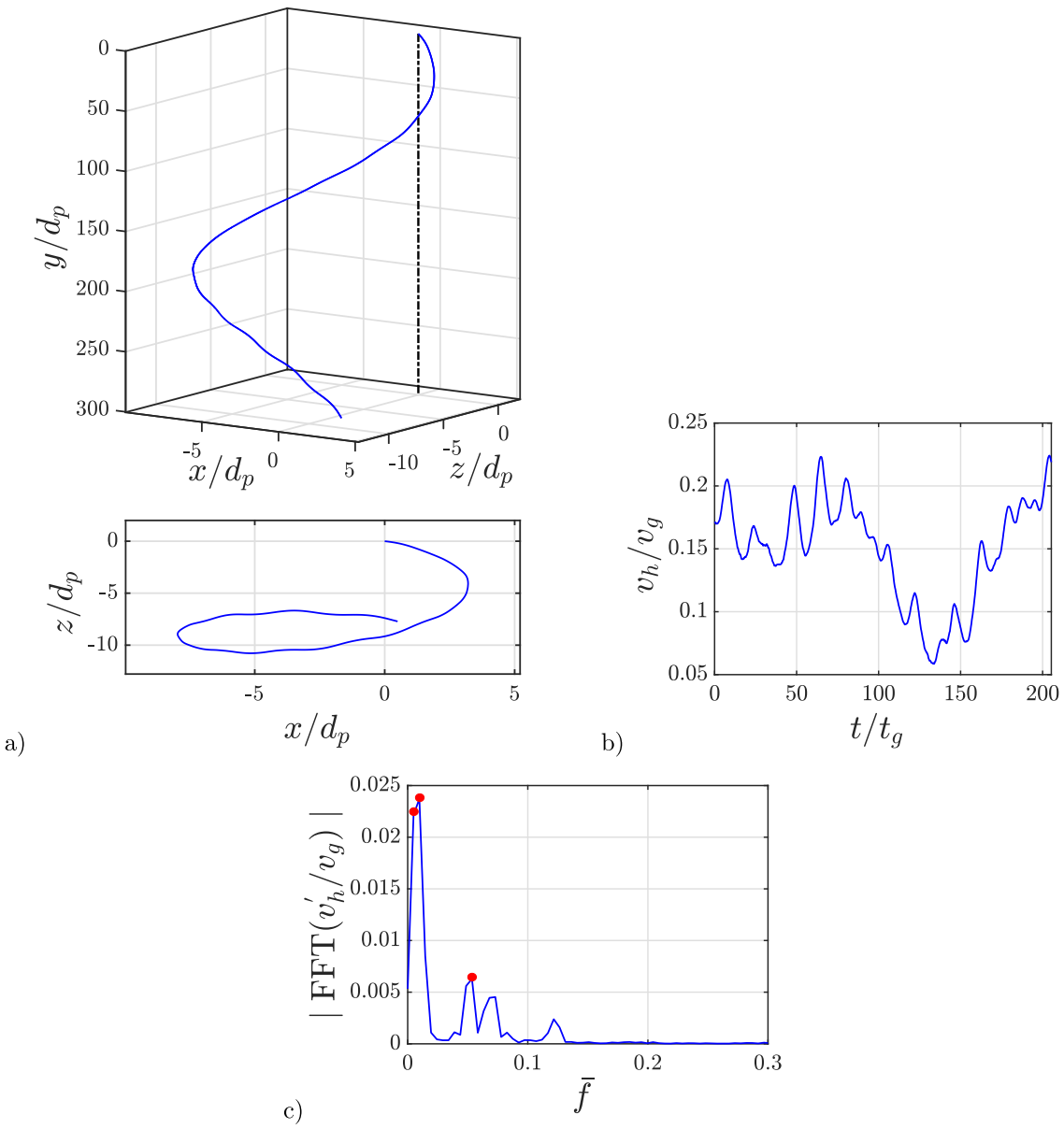

Fig. 14. (a) Helical/rotating trajectory for $\bar{\rho} = 3.191$ and $Ga = 208.42$ where half pitch and diameter of the helix are approximately $214d_p$ and $12d_p$ respectively, (b) Temporal variation of horizontal velocity, (c) Spectrum of the fluctuation of horizontal velocity (dominant peaks at 0.0048, 0.0097 and 0.053 indicated by red dots). (For interpretation of the references to colour in this figure legend, the reader is referred to the web version of this article.)

also multiple measurements with the same sphere at different water temperatures.

Steady oblique regime

Also for the dense cases, previous studies by JDB, ZD, VB and HW agree well with each other for the steady oblique regime. Hence, we decided not to probe this regime in detail. For the three measurement points indicated by the magenta squares in Fig. 13, we also observed a clear steady oblique regime.

Helical/rotating regime

On moving along lines H1 and H2, from the study of ZD we would first expect a high-frequency oscillating oblique regime for $Ga > 195$. This was, however, not the case in the present study. Instead we observed a direct transition to a **'helical/rotating'** regime in which the trajectory is oblique with low-frequency oscillations superimposed on a slow helical motion of the sphere. A typical trajectory is depicted in Fig. 14a. The half pitch and diameter of the helix are approximately $214d_p$ and $12d_p$, respectively. These values agree fairly well with those reported by ZD. In the spectrum depicted in Fig. 14c a dominant peak can be seen at $\overline{f} = 0.0048$, which corresponds to the slow helical motion of the sphere. Another peak can be seen at $\overline{f} = 0.053$, corresponding to the low-frequency oscillations superimposed on the rotation. Since it is not a perfect helix, it is named 'helical/rotating'. This regime was also observed by ZD for $212 \lesssim Ga \lesssim 240$ and $1.7 \lesssim \overline{\rho} \lesssim 10$. They characterized it as a bi-stable regime with the co-existence of a predominantly high-frequency oscillating oblique state and a chaotic state, where the symmetry plane of the oblique mode is fixed for the lower Ga range ("planar branch") and slowly rotates for the higher Ga range ("rotating branch"). In fact, the rotating branch was detected already by JDB for $Ga = 250$ and $\overline{\rho} = 5$ (their figure 20) and in the experiments of VB at $Ga = 212$ and $\overline{\rho} = 2.33$, though labelled as a chaotic state as no dominant oscillating frequency was found. In the present study, the measurements were repeated and the $(Ga, \overline{\rho})$ map (shown in Fig. 13) was thoroughly probed to investigate the Ga-extent and stability of this regime, and we always observe a *stable* rotating/helical regime for the cases considered (from $Ga = 205$ to Ga

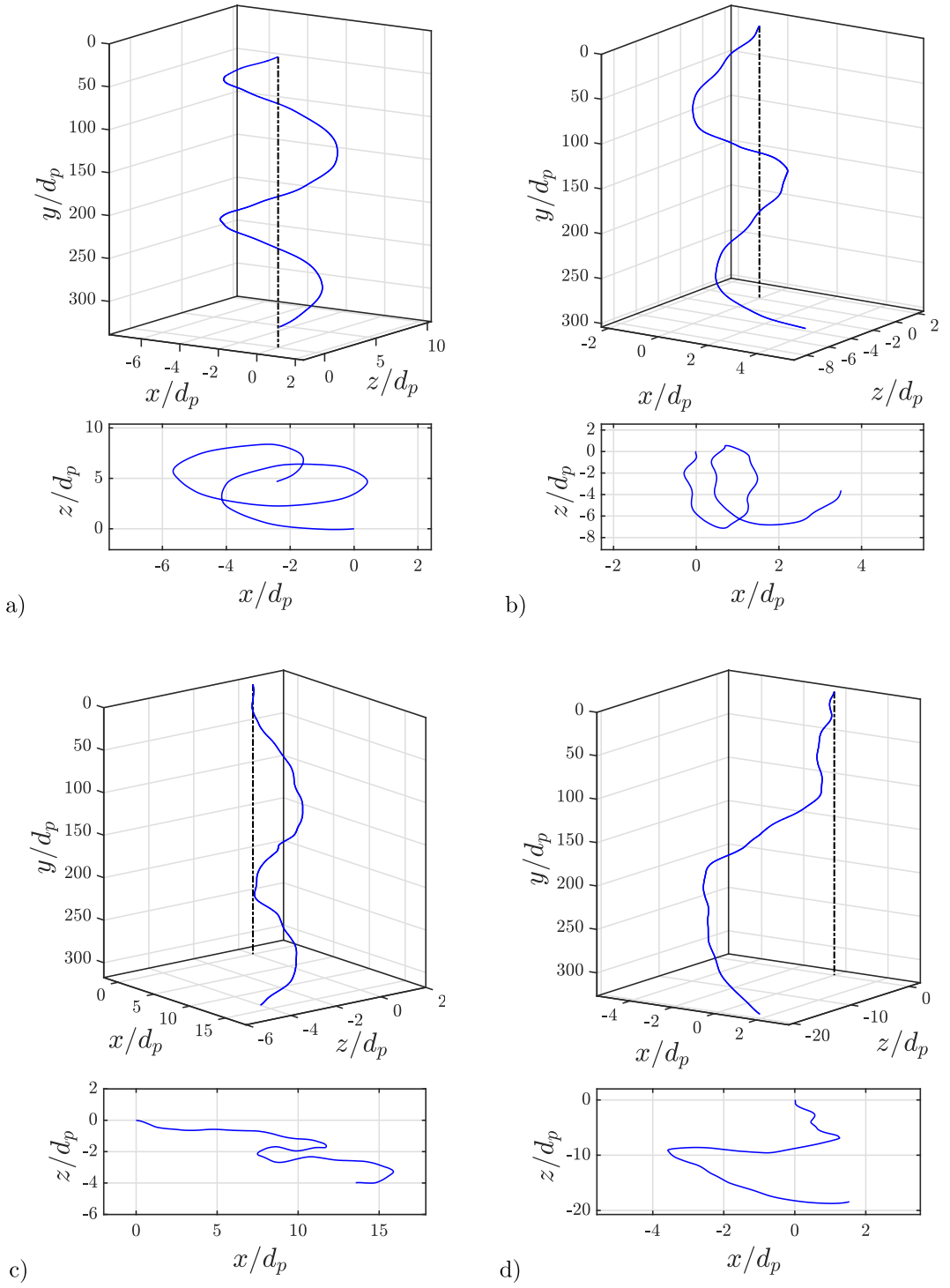

Fig. 15. (a) Helical/rotating trajectory with reduced pitch for $\bar{\rho}$ = 3.887 and Ga = 225.58 and dominant frequencies ($\bar{f}$) of 0.009 and 0.06, (b) Helical/rotating trajectory with reduced pitch and pronounced oscillations for $\bar{\rho}$ = 3.215 and Ga = 225.67 and dominant frequencies ($\bar{f}$) of 0.014 and 0.042, (c) Irregular helical/rotating trajectory $\bar{\rho}$ = 3.217 and Ga = 231.17, (d) Irregular helical/rotating trajectory $\bar{\rho}$ = 3.195 and Ga = 230.01.

= 231). Furthermore, for all measurement points in the range of Ga = 205 to 212, we never observed any signs of high-frequency oscillations near $\overline{f} \approx 0.18$ as reported by ZD, while our observed low-frequency oscillation peak at $\overline{f} \simeq 0.05$ is close to the secondary oscillation peak reported by them for this regime (their table 3).

The results from lines H1 and H2 are similar to each other, which contributes to confidence in the reliability of the present results. Moreover, this also shows that the heavy spheres ($\overline{\rho} \sim 3.19$ and 3.9) take a transition route that is clearly different from the moderately heavy spheres ($\overline{\rho} \sim 1.12$).

On increasing Ga within the rotating/helical regime, some intriguing characteristics were observed in the present study. For $Ga \gtrsim 222$ up till 231, the pitch of the helix decreased ($\approx 240 d_p$), to almost half of that observed for Ga between 205 and 215 (an example of such a phenomenon is shown in Fig. 15a). The oscillations also become much more pronounced (depicted in Fig. 15b), and in some cases the path

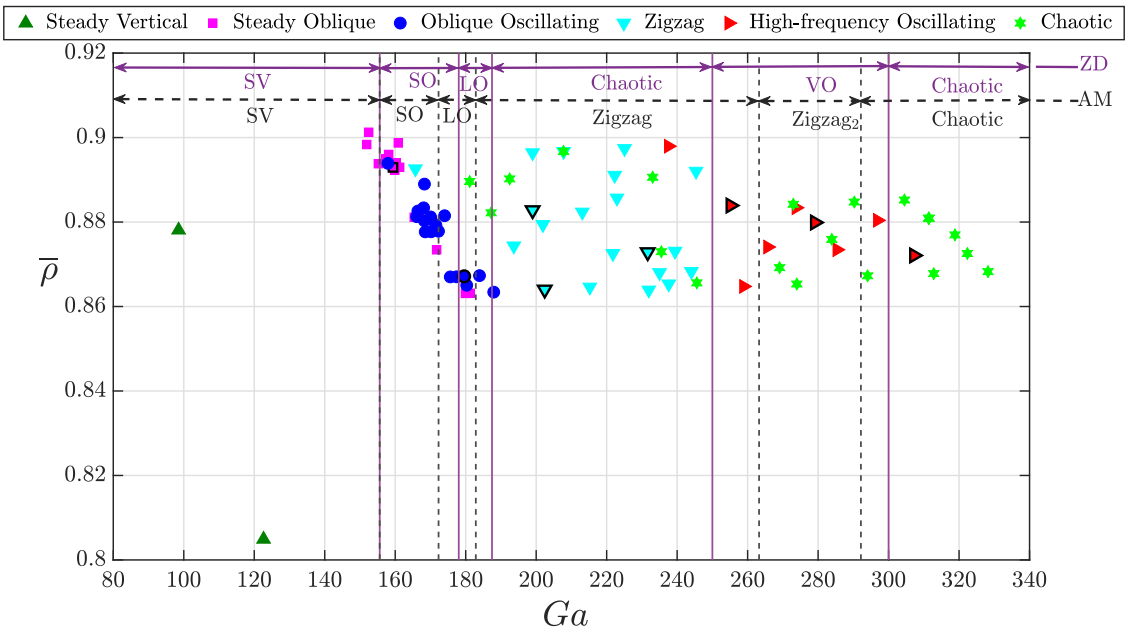

Fig. 16. Regime map updated along line ML with the results of the present study. The map presents a direct comparison with the maps of ZD and AM. The markers with a black outline are the cases for which the trajectories are shown. Violet and black vertical lines represent the thresholds of different regimes from the ZD and AM map respectively. SV — steady vertical, SO — steady oblique, LO — low-frequency oscillating oblique and VO — vertical oscillating. (For interpretation of the references to colour in this figure legend, the reader is referred to the web version of this article.)

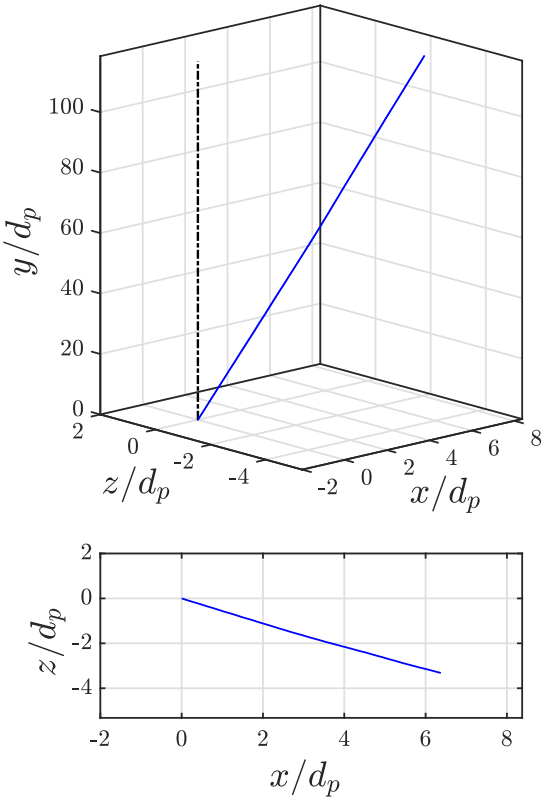

Fig. 17. Steady oblique trajectory for $\overline{\rho}$ = 0.892 and Ga = 159.36 rising at an angle of 3.47° with a mean vertical velocity ($\overline{v}_y/v_g$) and horizontal velocity ($\overline{v}_h/v_g$) of −1.38 and 0.084, respectively.

also shows slight deviations from the helical path indicating the onset of chaos. At $Ga \sim 231$, for one case we observe a helical/rotating regime (Fig. 15c) and in another case it is chaotic, indicating that somewhere around this Ga value the regime transitions to fully chaotic (Fig. 15d). This is in agreement with ZD, where they reported a critical value of Ga of 230–234 for $\overline{\rho}$ of 3–4 (their table 2). Beyond $Ga > 240$ we always observed a chaotic regime for all cases investigated, see Fig. 13.

3.3. Rising sphere — moderately light case ($\overline{\rho} \sim 0.87$)

In Fig. 16 the regime map obtained in the present study when moving along line ML is shown. This map directly compares the present results with the results of AM and ZD. The same map with the uncertainties included for every case is provided in Appendix B. For the moderately light case, 40 Polypropylene spheres were used and a total of 88 different measurements were performed. The measurements included that of different spheres and also multiple measurements with the same sphere but at different water temperatures.

Steady and oscillating oblique regimes

Earlier studies on a rising sphere show no disagreement with each other for the steady and oscillating oblique regimes. Hence these regimes serve as a good validation test for the present study to rule out the possible effect of perturbations originating from the vacuum-suction release mechanism. In the present study, both regimes were tested thoroughly, see Fig. 16, and the results are consistent with the studies of JDB, ZD and AM. The scatter of the data points in these regimes is consistent with the uncertainty in Ga (see Appendix B). Typical trajectories for the steady and oscillating oblique regimes are depicted in Fig. 17 and Fig. 18, respectively. For the investigated cases in the steady oblique regime, the angle with respect to the vertical varies between ∼ 2.9° and 6.1°. For the oscillating oblique regime, the angle varies between ∼ 2.2° and 6.3° and $\overline{f}$ ranges from ∼ 0.05 to 0.07. This again agrees with the previous studies.

Zigzag regime

Beyond the oscillating oblique regime we observed a low-frequency **'zigzag'** regime, which is also known as a characteristic mode of rising bubbles. Fig. 19a shows a typical trajectory of a sphere rising in a zigzag pattern. The oscillation amplitude is about 1 particle diameter (d_p), consistent with zigzag motions reported by JDB, ZD (for lower density ratios) and AM. Notice the small, regular and periodic, drift

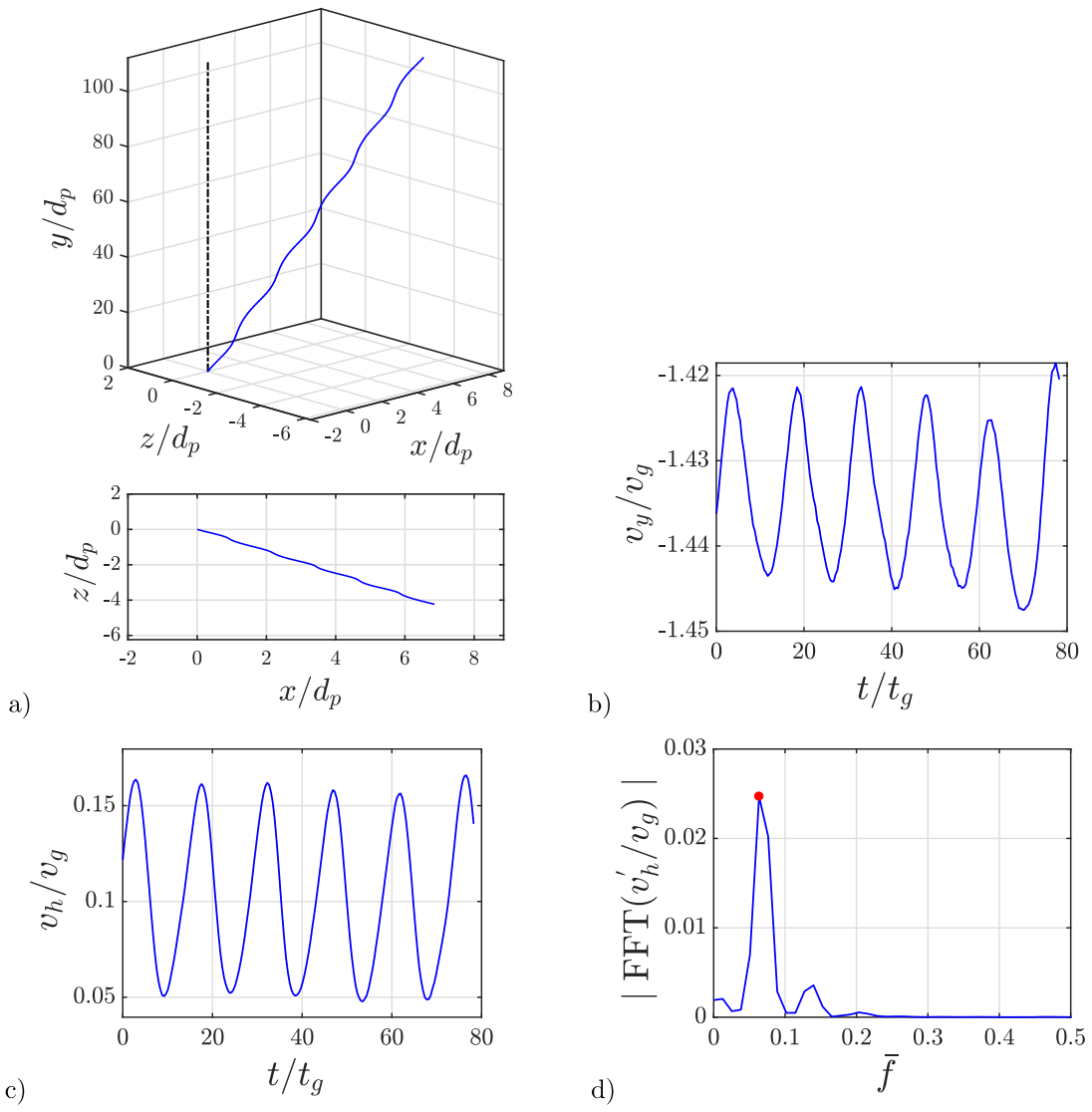

Fig. 18. (a) Oscillating oblique trajectory for $\overline{\rho}$ = 0.867 and Ga = 179.54 and with an average angle of 4.32° with respect to the vertical, a mean vertical velocity ($\overline{v}_y/v_g$) of −1.43 and mean horizontal velocity ($\overline{v}_h/v_g$) of 0.1, (b) Temporal variation of vertical velocity (amplitude of oscillation ~ $0.011v_g$), (c) Temporal variation of horizontal velocity (amplitude of oscillation ~ $0.05v_g$), (d) Spectrum of the fluctuation of horizontal velocity (with the red dot indicating the dominant peak at 0.063). (For interpretation of the references to colour in this figure legend, the reader is referred to the web version of this article.)

from the (x, z)-diagram in Fig. 19a, which may indicate that the drift is an intrinsic feature of this regime rather than the effect of residual motions inside the tank or due to imperfections of the sphere. From the spectrum, depicted in Fig. 19c, $\overline{f}$ is seen to be 0.043. The range in $\overline{f}$ as well as the corresponding range in St observed in the present study, are compared with the studies of JDB and AM in Table 3. Our ranges are in good agreement with their reported ranges, especially with the range in St of AM. JDB reported that the zigzag mode is planar and periodic (see their Fig.14). However, ZD pointed out that perfect planarity and periodicity is rather an exception. In contrast with this, the latest results of AM indicate again well-defined planar and periodic zigzag motion.

Beyond the oscillating oblique regime and in the Ga range of 200 to 250 and at $\overline{\rho}$ ~ 0.87, different studies disagree greatly with each other. JDB observed a zigzag regime up to Ga = 215. ZD did not observe a proper zigzag at this density ratio and reported a chaotic regime for Ga up to 250 and AM reported a zigzag regime for Ga up to 250. Experimentally, in this Ga range, HW observed zigzag motion for spheres only when $\overline{\rho}$ < 0.36 and VB never observed a proper zigzag regime. At this point, our results appear to agree best with AM. Note that we observed a few outliers with chaotic motion in this regime, as is evident from Fig. 16, which might be due to the possible presence of air voids in the sphere as discussed in Section 2.1. The zigzag regime is very sensitive to the sphere homogeneity as discussed by JDB (their figure 31). It is likely for this reason that VB only observed intermittent zigzag motion and not a full-fledged zigzag path. We also observed improper zigzag motions in a few investigated cases, see the examples shown in Fig. 20.

Table 3
$\overline{f}$ and St for zigzag regime and comparison with previous studies. Ranges for $\overline{\rho}$ and Ga are indicative for the outer bounds of the zigzag domain; the Ga range for which zigzag motion is observed depends on $\overline{\rho}$. Note that the range in $\overline{\rho}$ in the present study is limited as we only investigated polypropylene spheres in water.

Research article	$\overline{\rho}$	Ga	$\overline{f}$	St
Present study	0.86 to 0.9	190 to 250	0.022 to 0.047	0.017 to 0.032
JDB	< 1	175 to 215	0.023 to 0.035	–
AM	< 1	175 to 250	–	0.016 to 0.036

Bi-stable, high-frequency oscillating and chaotic regime

For 250 < Ga < 300 we observed a **'high-frequency oscillating'** regime similar to the high-frequency oscillating regime for the moderately heavy spheres discussed before. This regime bear resemblance

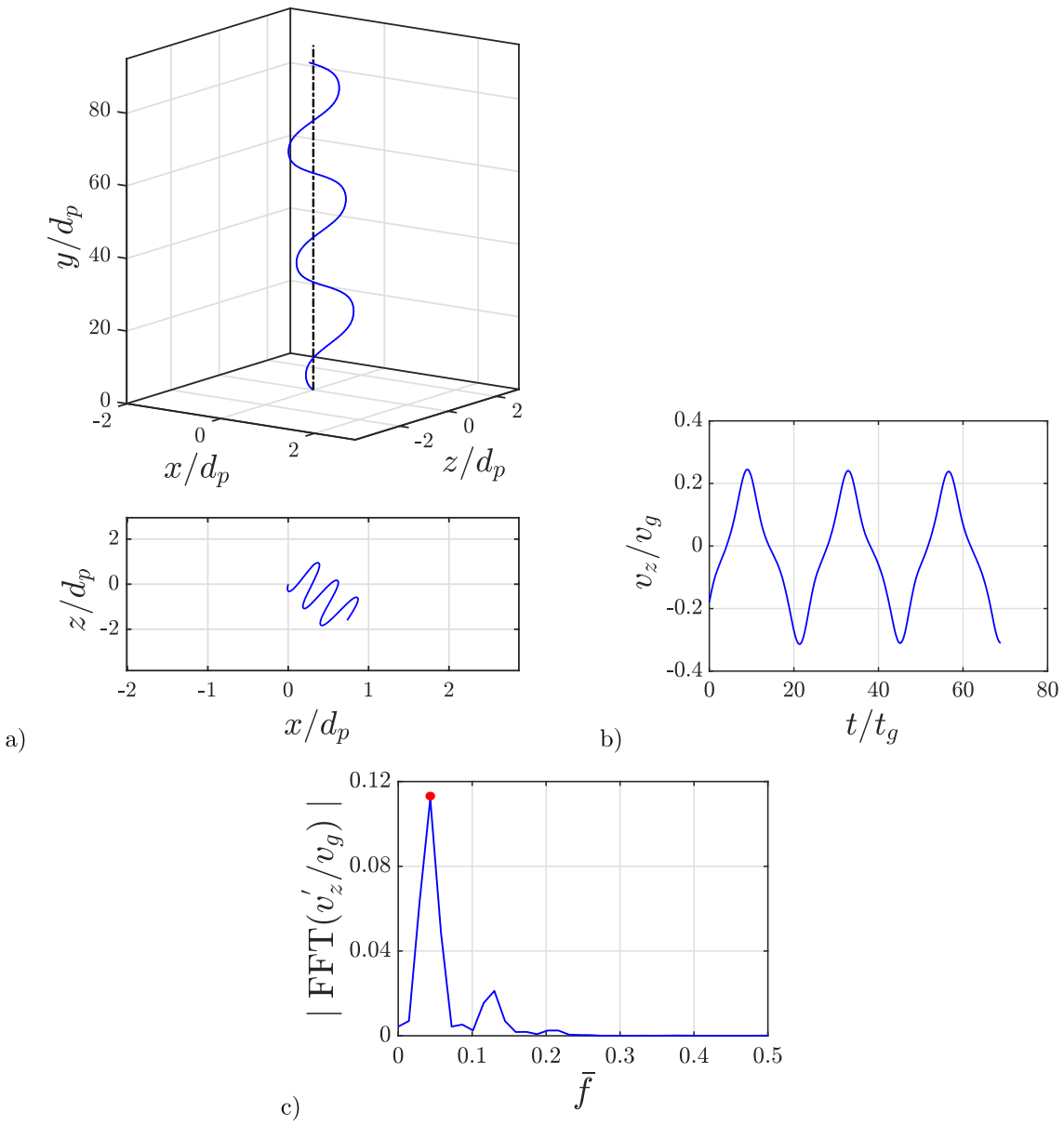

Fig. 19. (a) Zigzagging trajectory for $\overline{\rho}$ = 0.872 and Ga = 231.64, (b) Temporal variation of velocity in z-direction, (c) Spectrum of fluctuating velocity in z-direction (with the red dot indicating the dominant peak at 0.043). (For interpretation of the references to colour in this figure legend, the reader is referred to the web version of this article.)

with the zigzag regime discussed above, though with a more than three times higher oscillation frequency and a much smaller oscillation amplitude. Out of the 15 different experiments done in this Ga region, 6 were chaotic and 9 were high-frequency oscillating with $\overline{f}$ estimated to be around 0.14–0.15. There were cases where $\overline{f}$ was lower ($\sim$ 0.08) than the expected $\overline{f}$ for the high-frequency oscillating regime, but higher than that of the previously discussed oscillating oblique regime. It may be that these cases were under transition and had not reached their final state yet, and may had reached it when they would have been tracked over a larger distance. This speculation will be further corroborated below. This regime appears to coexist with the chaotic regime and hence we deem it as bi-stable in the present study. A typical trajectory, along with the velocity evolution and spectra, is depicted in Fig. 21. Notice the small lateral drift. Similar to the drift observed for the zigzag trajectory in Fig. 19, we are not completely sure whether this drift is an intrinsic feature of this regime or a spurious phenomenon due to, for example, sphere imperfections.

ZD characterized this regime as fully stable and strictly vertical (2D) and called it 'vertical oscillating' and AM characterized this regime as a fully stable high-frequency drifting regime (3D) and called it 'ZZ_2'. AM reported the emergence of this regime after the sphere had travelled approximately $330d_p$ for $\overline{\rho}$ = 0.75 and Ga = 275, but in the present study, the sphere enters our field of view after approximately $187.5d_p$. It may thus be very well that in a few of our cases in this Ga region, the sphere was still under transition as speculated above and may have ended up in the high-frequency oscillating state if it could have continued to rise. In some other cases we observed a transition from chaos to a high-frequency oscillating state and back to chaos again (Fig. 22a), while again in other cases we observed a chaotic regime with strong imprints of high-frequency oscillations (Fig. 22b). This is indicative of a bi-stable nature. In Fig. 16 these points are characterized as high-frequency oscillating (red markers) and not chaotic since the imprints of the former are evidently seen. We also observed fully chaotic regimes which had no evident imprints of high-frequency oscillations. Hence, for $Ga \sim$ 250 to 300 both red and green markers are present in Fig. 16 and we qualify this entire Ga range as a bi-stable regime.

Similar to the zigzag regime, also the high-frequency oscillating regime might be sensitive to inhomogeneity in mass distribution within

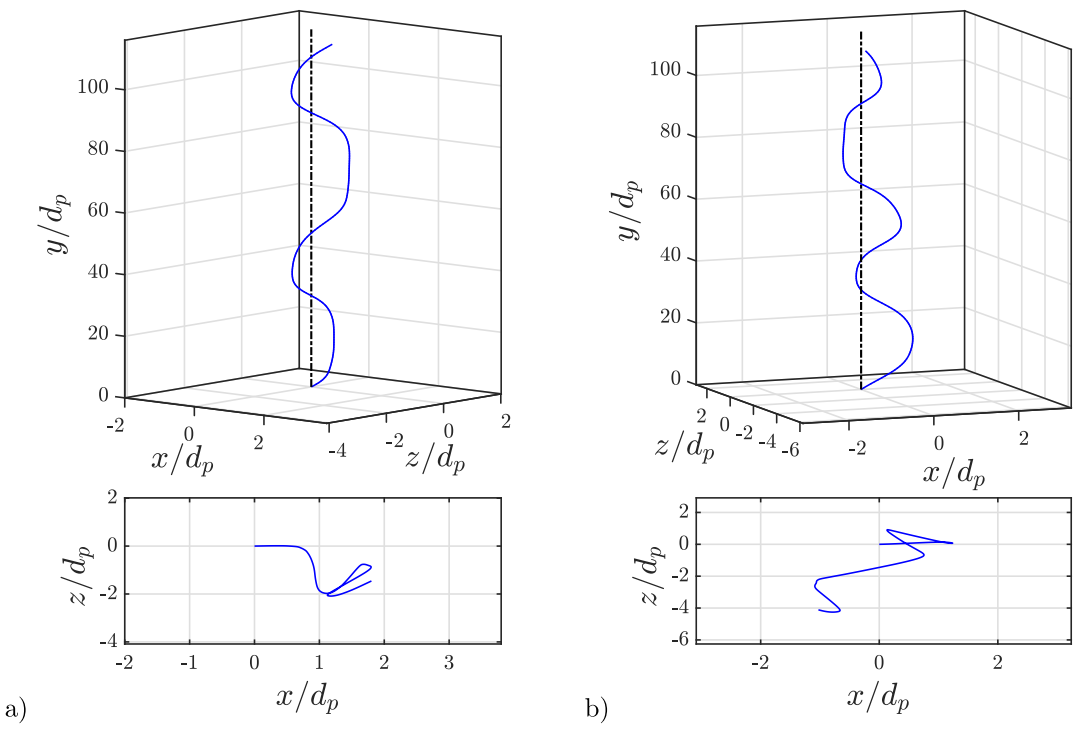

Fig. 20. Examples of improper zigzag trajectories at (a) $\overline{\rho}$ = 0.864 and Ga = 202.42, and (b) $\overline{\rho}$ = 0.882 and Ga = 198.98.

the sphere. It is left for future research to investigate to what extent this effect was present in the current experiments. For this it would be desired to repeat the experiments in this regime for other high-quality spheres that are manufactured preferably in a different manner.

Finally, when moving along line ML, for $Ga > 300$ we observed always a chaotic regime (with only one exception), consistent with results of ZD and AM.

The three velocity components (v_x, v_y and v_z) are plotted in a velocity diagram in Fig. 23 for all the regimes observed when moving along line ML. This plot shows that with transition to chaos, the area occupied in 3D space increases, signifying an increase in lateral velocity excursions of the sphere. For the cases shown, we again estimated the fraction of work by gravity that is lost to horizontal sphere motion (η), see the values of η in Fig. 23. The maximum value of η is observed for the zigzagging regime ($2.1 \cdot 10^{-2}$) as opposed to the steady oblique regime ($1.9 \cdot 10^{-2}$) for the moderately heavy cases. This is due to the very large oscillation amplitude that is seen for the zigzagging regime (see Fig. 19). However, as for the falling cases discussed before, η is small and hence negligible effect may be expected from horizontal sphere motions on the drag coefficient (C_d).

3.4. Drag coefficient

The variation of the drag coefficient (C_d) with Reynolds number (Re) for the falling and rising spheres are shown in Fig. 24 and Fig. 25, respectively. We computed C_d by assuming a balance between the steady drag force and the net gravity force according to Horowitz and Williamson (2010) and Auguste and Magnaudet (2018):

$$C_d = \frac{4}{3}\frac{Ga^2}{Re^2}, \tag{4}$$

where Re is based on the mean vertical terminal settling velocity. In both plots the data from the experiments are compared with that of a fixed sphere, represented by Abraham's drag correlation (Abraham, 1970) given by Eq. (5a) and the correlation of Brown and Lawler (2003) given by Eq. (5b):

$$C_d = \left(\sqrt{\frac{24}{Re}} + 0.5407\right)^2, \qquad 0 \lesssim Re \lesssim 5000, \tag{5a}$$

$$C_d = \frac{24}{Re}\left(1 + 0.150Re^{0.681}\right) + \frac{0.407}{1 + 8710Re^{-1}}, \qquad Re < 2 \times 10^5. \tag{5b}$$

As already anticipated based on our previous evaluation of η, for both the rising and falling cases the drag coefficient is not significantly different from the drag coefficient for a fixed sphere when taking the measurement uncertainty into account. The accuracy of C_d is set by the accuracy of the measured mean vertical velocity, the mass of the sphere, the sphere diameter and, to a minor extent, the temperature as the fluid density depends on it. The accuracy of Re depends on the measured mean vertical velocity, the sphere diameter, and the temperature, as both the kinematic viscosity and the fluid density depend on it. Note that the relative uncertainty in Re is comparatively small with respect to the uncertainty in C_d. Details of the uncertainty analysis can be found in the supplementary material. For the falling spheres, our results agree with the findings of HW, who reported that for all non-vibrating spheres (including all spheres with $\overline{\rho} > 1$), the drag coefficient did not significantly change relative to a fixed sphere. For the rising spheres, our results agree with VBL and AM as they found only a significant enhancement of the drag coefficient for very low $\overline{\rho}$ ($\overline{\rho}$ = 0.02 for VBL and $\overline{\rho} \lesssim 0.3$ for AM), which is well below our investigated range of density ratios.

4. Summary and conclusions

Below our most important findings are summarized and compared with previous studies to draw points of consensus and disagreements:

1. For the moderately heavy spheres ($\overline{\rho} \sim 1.12$), the steady oblique and oscillating oblique regimes were observed consistently over a Ga range of ~ 160–190, in agreement with the simulation results of ZD and JDB. These two regimes were also observed in experiments by VB and the steady oblique regime was observed by HW.
   On increasing Ga for the moderately heavy spheres ($\overline{\rho} \sim 1.12$), for $250 < Ga < 300$ a high-frequency oscillating regime was observed in the present study. This regime was reported by

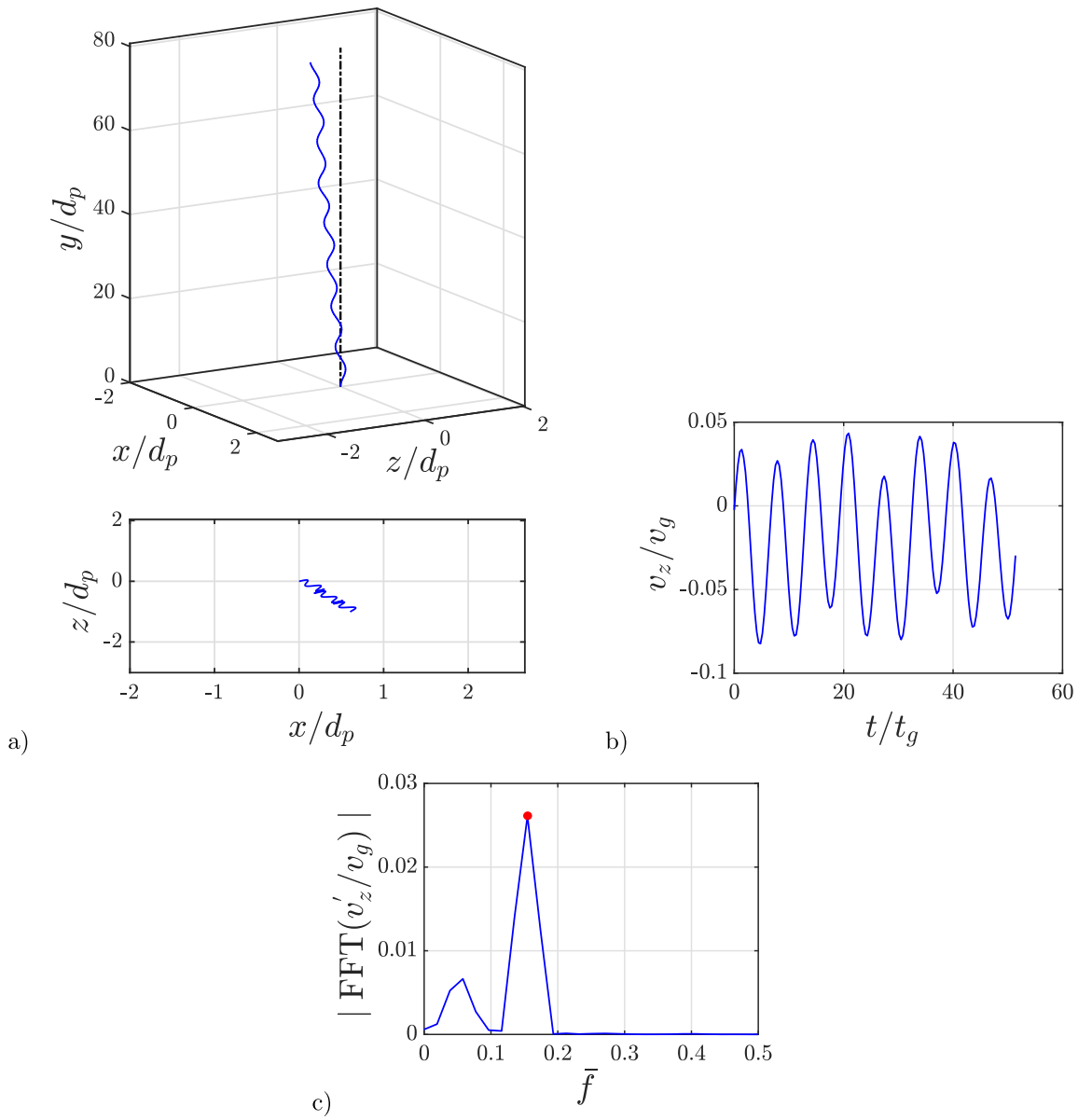

Fig. 21. (a) High-frequency oscillating trajectory for $\overline{\rho}$ = 0.879 and Ga = 279.11, (b) Temporal variation of velocity component in z-direction, (c) Spectrum of the fluctuation of velocity component in z-direction (with the red dot indicating the dominant peak at 0.154). (For interpretation of the references to colour in this figure legend, the reader is referred to the web version of this article.)

JDB only for rising spheres, but by ZD also for falling spheres in the same Ga range at this particular density ratio. To our knowledge, this is the first time such a regime has been observed experimentally. In the present study this entire region of 250 < Ga < 300 is categorized as bi-stable as in JDB for rising cases (see their figures 26 and 27), characterized by the coexistence of a high-frequency oscillating regime as well as a chaotic regime. ZD characterized this region as partly bi-stable as bi-stable behaviour was observed by them only for three cases. Hence, the present study does not agree with JDB for 250 < Ga < 300, but we agree with the map of ZD, except that in the present study the high-frequency oscillating regime is characterized as a fully bi-stable one.

2. For the heavy spheres ($\overline{\rho} \sim$ 3.19 and 3.9) and the range of Ga considered, we initially observed a steady oblique regime, then a helical/rotating regime, and, upon increasing Ga further, transition into a chaotic regime. This disagrees with the findings of ZD and JDB as they reported also the presence of a high-frequency oscillating oblique regime directly after the steady oblique regime on increasing Ga. However, repeated measurements were made and we did never observe such a regime. The helical/rotating regime was reported by ZD, but it occurred after transition from the high-frequency oscillating oblique regime. Moreover, they characterized the helical/rotating regime as a bi-stable one with the co-existence of a chaotic regime. We conducted an extensive measurement campaign for the helical/rotating regime, but we never observed signs of bi-stability. Instead, measured sphere trajectories in the helical/rotating regime were well repeatable and stable. This regime was also observed by JDB and VB for one case, albeit they qualified it as a chaotic mode as no clear peaks could be observed in the frequency spectrum. Our measured frequency spectra clearly show the presence of a main, low-frequency, peak, similar to that reported by ZD and corresponding to the slow helical motion, and the presence of a smaller, higher-frequency, peak, related to the oscillations on top of the helical motion. For $Ga \gtrsim 222$, we observed that the pitch of the helix reduces to almost half

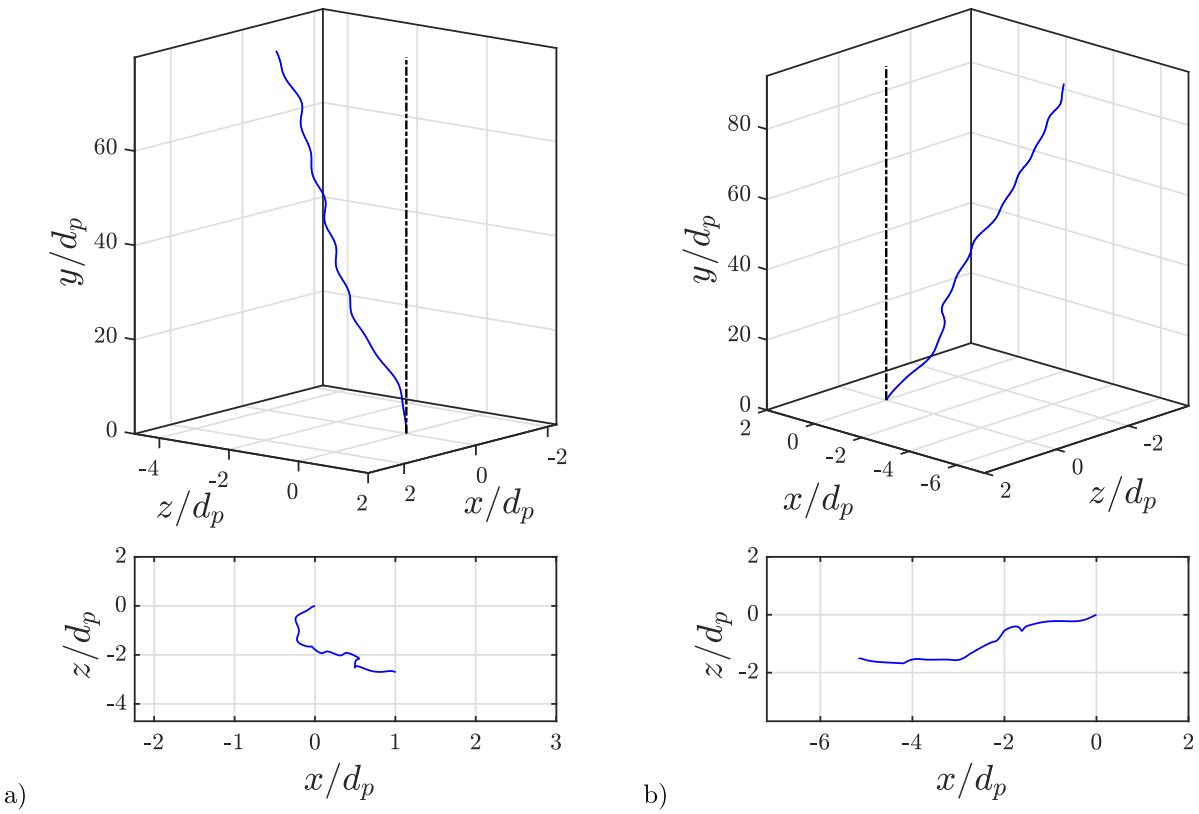

Fig. 22. (a) Trajectories in bi-stable regime for (a) $\overline{\rho}$ = 0.872 and Ga = 307.23, and (b) $\overline{\rho}$ = 0.883 and Ga = 255.16.

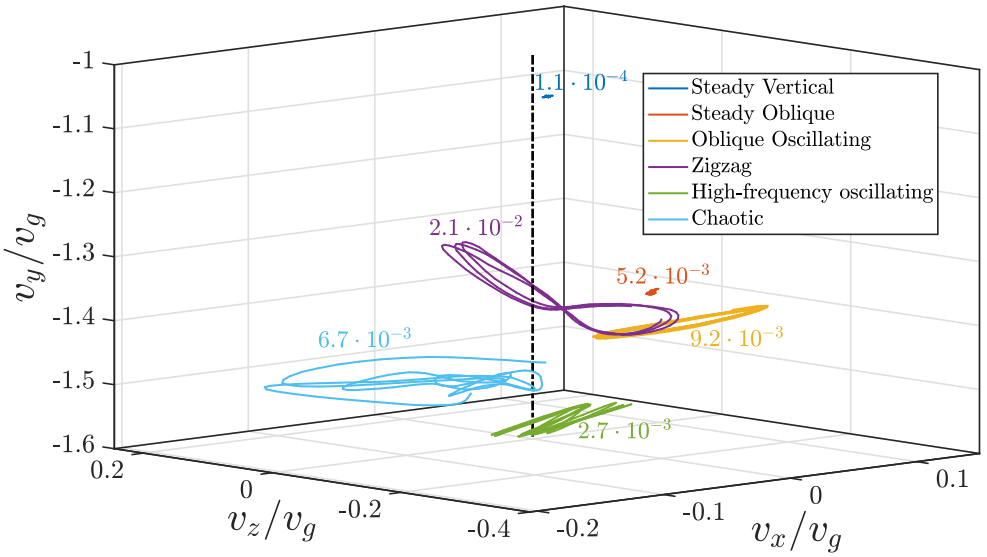

Fig. 23. 3D velocity plot for all the regimes along line ML, with Ga and $\overline{\rho}$ for each regime corresponding to: Steady Vertical — Ga = 98.53 and $\overline{\rho}$ = 0.878, Steady Oblique — Ga = 159.36 and $\overline{\rho}$ = 0.892, Oscillating Oblique — Ga = 179.54 and $\overline{\rho}$ = 0.867, Zigzag — Ga = 231.64 and $\overline{\rho}$ = 0.872, High-frequency oscillating — Ga = 279.1 and $\overline{\rho}$ = 0.879, Chaotic — Ga = 307.23 and $\overline{\rho}$ = 0.872. The numbers in the plot are the values of η (see Eq. (3c)) for each regime.

of that observed for $Ga \lesssim 222$ and oscillations become more pronounced. On increasing Ga further, close to $Ga \sim 230$, we observe transition to the chaotic regime. This Ga value for transition matches very well with the critical Ga value mentioned by ZD.

3. For moderately light spheres, a single $\overline{\rho}$ (~ 0.87) was investigated for a wide range of Ga. Here, we have a better basis for comparison as three maps were drafted by two different research groups with a different numerical method and code employed for their study. Our results for the steady oblique and oscillating oblique regimes agree well with all the three studies and also with the experimental study of VB.

Post the oscillating oblique regime, the rising spheres exhibited zigzag motion. The transition from an oscillating oblique to a zigzag regime at $\overline{\rho} \sim 0.87$ is only reported by AM and JDB, but not by ZD at this density ratio. We observed the zigzag regime immediately after the oscillating oblique regime up to $Ga \sim 250$, which is in good agreement with AM. This regime is known

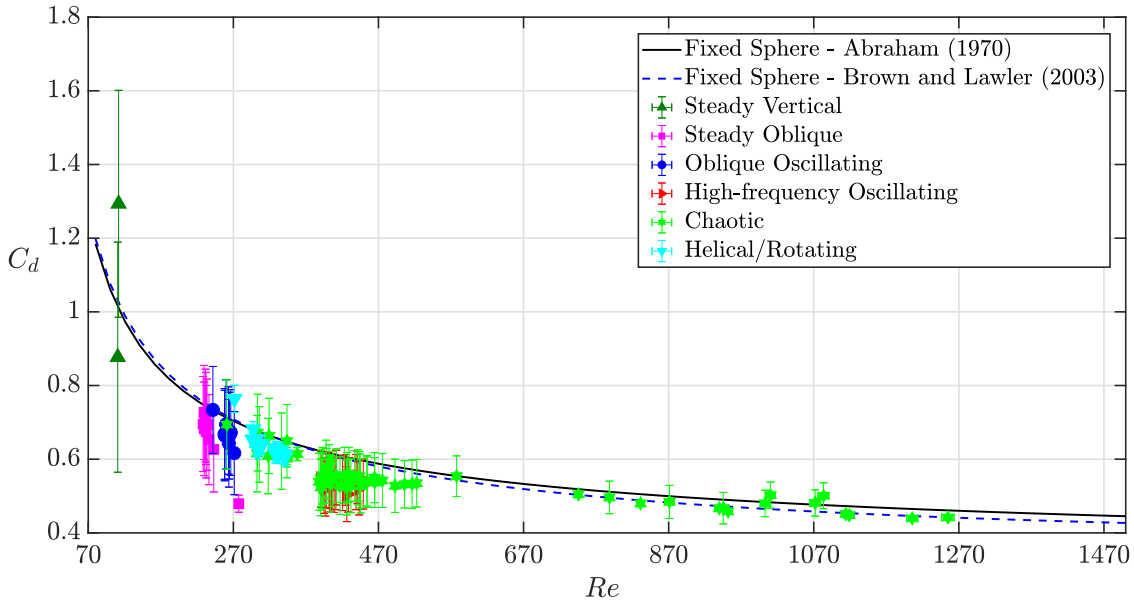

Fig. 24. C_d as function of Re for all falling sphere cases (the fixed sphere curves are the correlations proposed by Abraham (1970) (Eq. (5a)) and Brown and Lawler (2003) (Eq. (5b)).

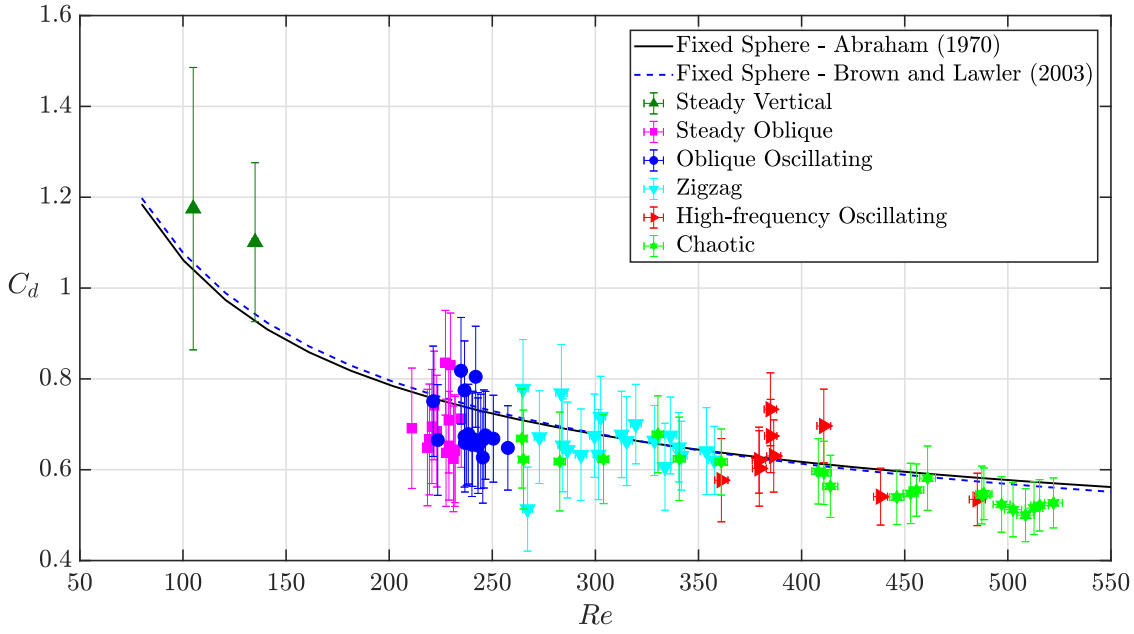

Fig. 25. C_d as function of Re for all rising sphere cases (the fixed sphere curves are the correlations proposed by Abraham (1970) (Eq. (5a)) and Brown and Lawler (2003) (Eq. (5b)).

to be sensitive to inhomogeneity in mass distribution within the sphere, which may explain why in the present study a few improper zigzags and also some chaotic outliers were observed. For $250 > Ga > 300$, the rising spheres were in the high-frequency oscillating regime similar to what we observed for the moderately heavy cases at $\overline{\rho} \sim 1.12$. Again, as far as we know, this is the first time such a regime has been observed experimentally. Furthermore, this regime coexists with the chaotic regime thereby making it bi-stable. In some cases, the sphere was in transition to the high-frequency state, where a state of intermediate oscillations was seen. This regime was also observed by JDB and they also reported a bi-stable behaviour. ZD characterized this regime as fully stable and strictly vertical (2D) and AM characterized it as a high-frequency drifting regime (3D). Based on the present results, we qualify this regime as a bi-stable chaotic/high-frequency oscillating regime.

4. The results for the drag coefficient of the falling and rising spheres are not significantly different from the drag coefficient for a fixed sphere. This is in agreement with the previous studies for the currently investigated range of density ratios. The scatter in our results fall within the measurement uncertainty of C_d.

Beyond the steady oblique regime, our results do not agree with the experiments of HW. The reason for this is unclear, but, as already discussed in the introduction, previous studies also disagree largely with HW. However, our results are in good agreement with the experimental study of VB. Although VB did not cover a wide range of Ga as in the present experimental campaign and rather focused on specific regimes, all the regimes observed by VB were also observed in the present study.

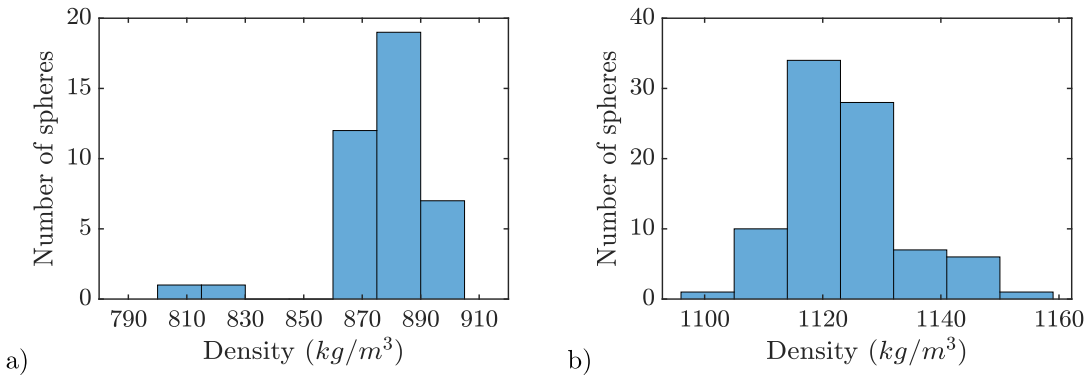

Fig. 26. (a) Polypropylene spheres (total number — 40, density specified by supplier = 870 kg/m^3. Mean density = 876.55 kg/m^3, standard deviation = 17.25 kg/m^3, (b) Nylon spheres (total number — 87, density specified by supplier = 1120 kg/m^3). Mean density = 1123.69 kg/m^3, standard deviation = 9.98 kg/m^3.

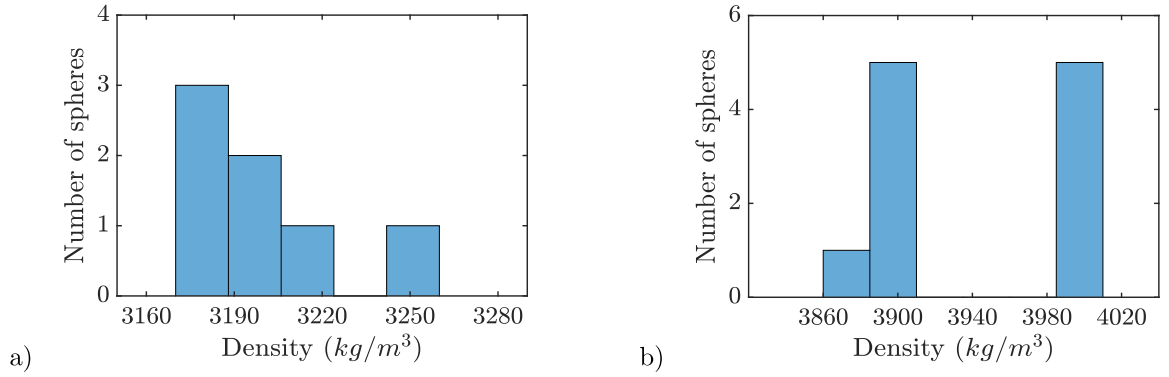

Fig. 27. (a) Silicon Nitride spheres (total number — 7, density specified by supplier = 3190 kg/m^3). Mean density = 3201.36 kg/m^3, standard deviation = 28.17 kg/m^3, (b) Aluminium Oxide spheres (total number — 11, density specified by supplier = 3900 kg/m^3). Mean density = 3940.91 kg/m^3, standard deviation = 56.09 kg/m^3.

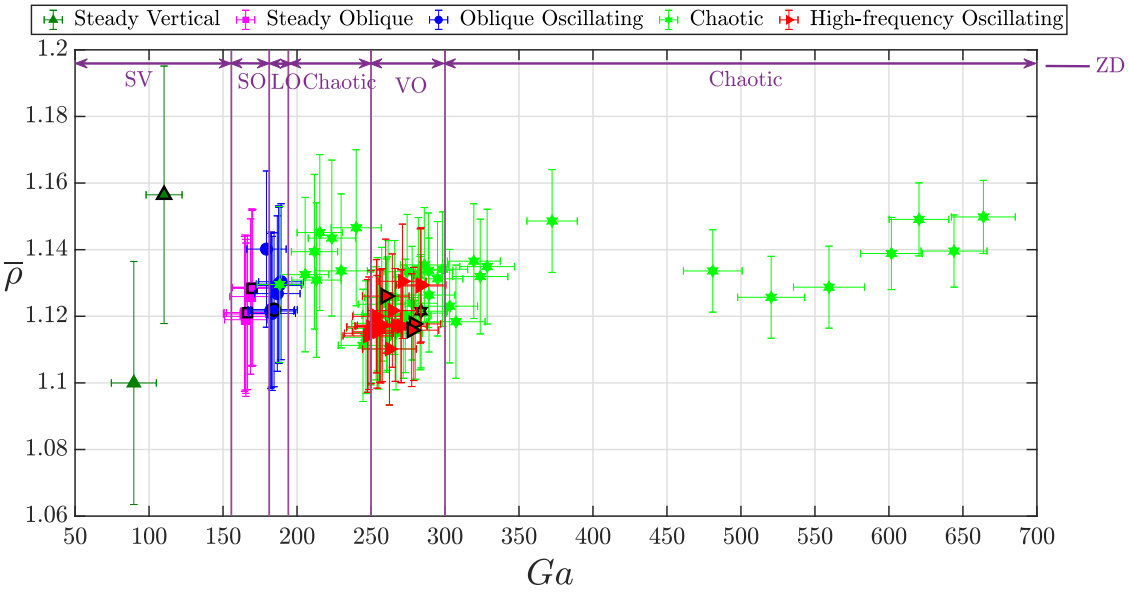

Fig. 28. Regime map updated along line MH with the results of the present study including uncertainties. Annotations are the same as in Fig. 5.

In the zigzag regime, VB only observed improper zigzag trajectories, which we also observed in a few cases in the present study. Our results agree very well with AM for the rising spheres and fairly well with ZD and JDB for both the rising and falling spheres. It remains puzzling why in the updated regime map of ZD, the zigzag regime was detected only up to $\overline{\rho} = 0.5$ in contrast with the older map of JDB, the map of AM and our current findings. Moreover, for the heavy cases, we observed a direct transition from the steady oblique into the helical/rotating regime, while JDB and ZD both report the presence of an intermediate high-frequency oblique oscillating regime.

The bi-stable regimes found in the present study need to be cross-verified by performing similar experiments on a larger tank so that the sphere can be tracked over a considerably larger distance. Preferably

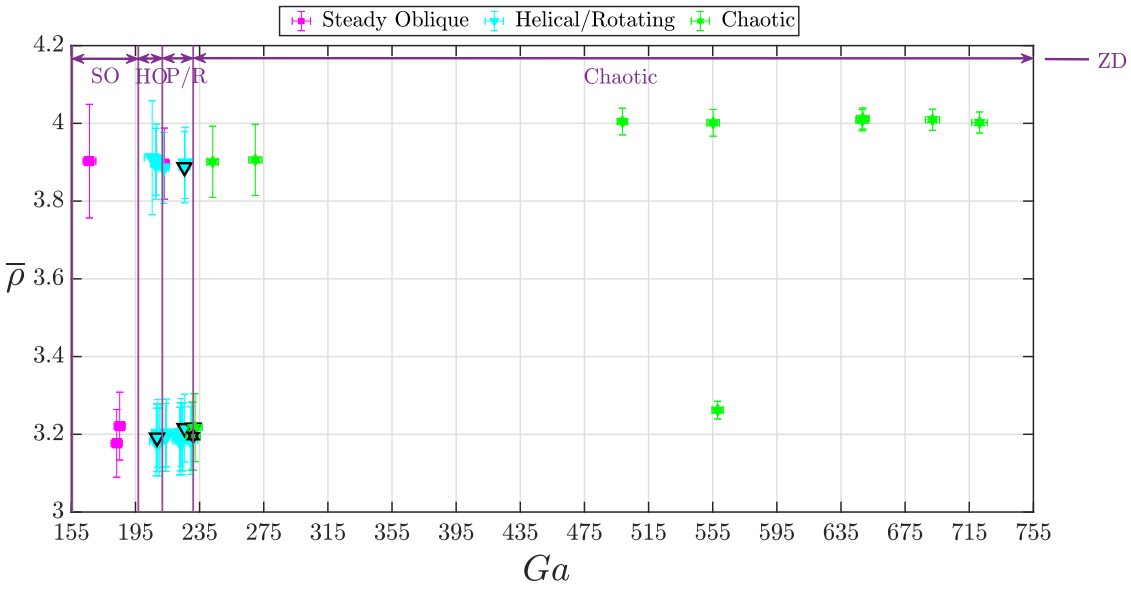

Fig. 29. Regime map updated along line H1 and H2 with the results of the present study including uncertainties. Annotations are the same as in Fig. 13.

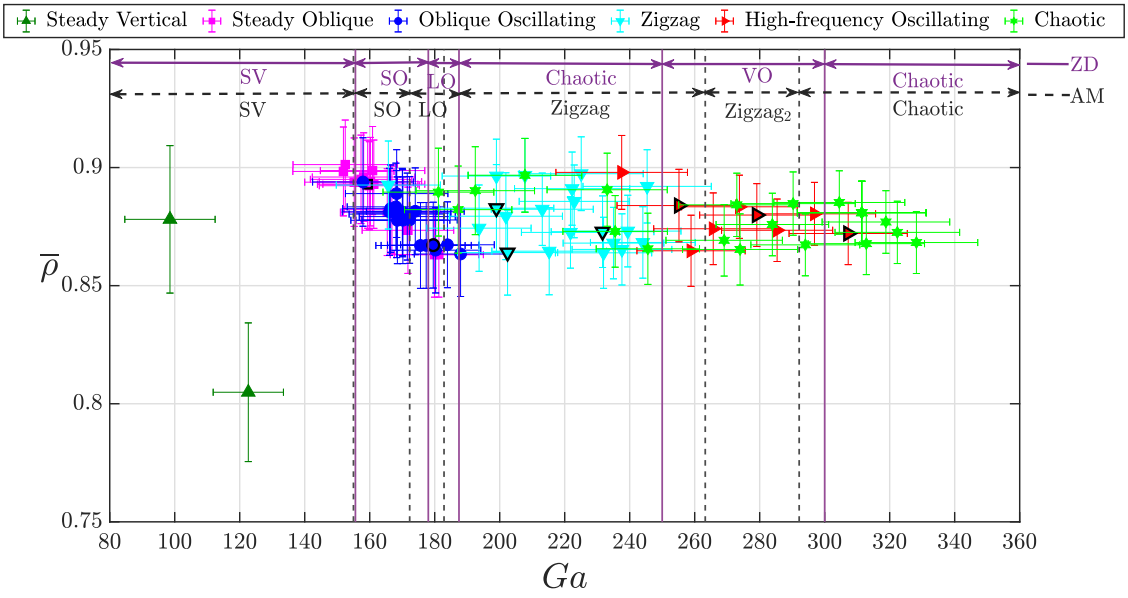

Fig. 30. Regime map updated along line ML with the results of the present study including uncertainties. Annotations are the same as in Fig. 16.

other high-quality spheres should be used too, manufactured in a different manner and with a high degree of homogeneity in mass distribution within the sphere.

There are still a lot of interesting regimes that have not been covered yet by experiments, mainly because we did not investigate density ratios for $\overline{\rho} < 0.5$. Future experimental studies should aim at covering these low density ratios for rising spheres. This will pave the way for a comprehensive full (Ga, $\overline{\rho}$) regime map, which can be created by combining results from different experimental and numerical studies.

Funding

This research did not receive any specific grant from funding agencies in the public, commercial, or not-for-profit sectors. It was conducted as part of the MSc thesis project of the first author at TU Delft.

CRediT authorship contribution statement

Shravan K.R. Raaghav: Conceptualization, Methodology, Software, Validation, Formal analysis, Investigation, Resources, Data curation, Writing – original draft, Visualization, Project administration. **Christian Poelma:** Methodology, Writing – review & editing, Supervision. **Wim-Paul Breugem:** Conceptualization, Methodology, Resources,Writing – review & editing, Supervision, Project administration.

Declaration of competing interest

The authors declare that they have no known competing financial interests or personal relationships that could have appeared to influence the work reported in this paper.

Acknowledgements

The authors would like to express their gratitude to Jan Graafland, Edwin Overmars and Jasper Ruijgrok for their help with the experiments and to Mike van Meerkerk for making the camera calibration code available. We also thank the two anonymous reviewers for their comments, which helped to improve the manuscript.

Appendix A. Density variation of precision spheres

See Figs. 26 and 27.

Appendix B. Regime maps with uncertainties

See Figs. 28–30.

Appendix C. Supplementary material

Supplementary material related to this article can be found online at https://doi.org/10.1016/j.ijmultiphaseflow.2022.104111.

References

Abraham, F., 1970. Functional dependence of drag coefficient of a sphere on Reynolds number. Phys. Fluids 13 (8), 2194–2195.
Auguste, F., Magnaudet, J., 2018. Path oscillations and enhanced drag of light rising spheres. J. Fluid Mech. 841, 228–266.
Brown, P.P., Lawler, D.F., 2003. Sphere drag and settling velocity revisited. J. Environ. Eng. 129 (3), 222–231.
Daniel, B., Dufresne, E., 2008. The matlab particle tracking code repository.
Di Felice, R., Parodi, E., 1996. Wall effects on the sedimentation velocity of suspensions in viscous flow. AIChE J. 42 (4), 927–931.
Ellingsen, K., Risso, F., 2001. On the rise of an ellipsoidal bubble in water: oscillatory paths and liquid-induced velocity. J. Fluid Mech. 440, 235–268.
Ern, P., Risso, F., Fabre, D., Magnaudet, J., 2012. Wake-induced oscillatory paths of bodies freely rising or falling in fluids. Annu. Rev. Fluid Mech. 44, 97–121.
Fabre, D., Auguste, F., Magnaudet, J., 2008. Bifurcations and symmetry breaking in the wake of axisymmetric bodies. Phys. Fluids 20 (5), 051702.
Fabre, D., Tchoufag, J., Magnaudet, J., 2012. The steady oblique path of buoyancy-driven disks and spheres. J. Fluid Mech. 707, 24–36.
Fernandes, P.C., Risso, F., Ern, P., Magnaudet, J., 2007. Oscillatory motion and wake instability of freely rising axisymmetric bodies. J. Fluid Mech. 573, 479–502.
Ghidersa, B., Dušek, J., 2000. Breaking of axisymmetry and onset of unsteadiness in the wake of a sphere. J. Fluid Mech. 423, 33–69.
Hartley, R., Zisserman, A., 2003. Multiple View Geometry in Computer Vision. Cambridge University Press.
Horowitz, M., Williamson, C.H.K., 2010. The effect of Reynolds number on the dynamics and wakes of freely rising and falling spheres. J. Fluid Mech. 651, 251–294.
Jenny, M., Dušek, J., Bouchet, G., 2004. Instabilities and transition of a sphere falling or ascending freely in a Newtonian fluid. J. Fluid Mech. 508, 201–239.
Karamanev, D.G., Chavarie, C., Mayer, R.C., 1996. Dynamics of the free rise of a light solid sphere in liquid. AIChE J. 42 (6), 1789–1792.
Karamanev, D.G., Nikolov, L.N., 1992. Free rising spheres do not obey Newton's law for free settling. AIChE J. 38 (11), 1843–1846.
Maas, H.G., Gruen, A., Papantoniou, D., 1993. Particle tracking velocimetry in three-dimensional flows. Exp. Fluids 15 (2), 133–146.
Magnaudet, J., 1997. The forces acting on bubbles and rigid particles. In: Proc. ASME Fluids Eng. Div. Summer Meeting, Vancouver, Canada, Paper 97-3522. ASME.
Mathai, V., Zhu, X., Sun, C., Lohse, D., 2018. Flutter to tumble transition of buoyant spheres triggered by rotational inertia changes. Nature Commun. 9 (1), 1792.
Mittal, R., 1999. Planar symmetry in the unsteady wake of a sphere. AIAA J. 37 (3), 388–390.
Natarajan, R., Acrivos, A., 1993. The instability of the steady flow past spheres and disks. J. Fluid Mech. 254, 323–344.
Newton, I., 1726. In: Cohen, I.B., Whitman, A. (Eds.), Philosophia Naturalis Principia Mathematica, third edn. University of California Press, 1999.
Nicholas, O.T., Xu, H., Bodenschatz, E., 2006. A quantitative study of three-dimensional Lagrangian particle tracking algorithms. Exp. Fluids 40 (2), 301–303.
Ormières, D., Provansal, M., 1999. Transition to turbulence in the wake of a sphere. Phys. Rev. Lett. 83 (1), 80.
Raaghav, S.K.R., 2019. Path Instabilities of a Rising Or Falling Sphere in a Fluid At Rest - an Experimental Study. (MSc thesis). Delft University of Technology.
Savitzky, A., Golay, M.J., 1964. Smoothing and differentiation of data by simplified least squares procedures. Anal. Chem. 36 (8), 1627–1639.
Soloff, S.M., Adrian, R., 1997. Distortion compensation for generalized stereoscopic particle image velocimetry. Meas. Sci. Technol. 8 (12), 1441.
Tomboulides, A.G., Orszag, S.A., 2000. Numerical investigation of transitional and weak turbulent flow past a sphere. J. Fluid Mech. 416, 45–73.
Toupoint, C., Ern, P., Roig, V., 2019. Kinematics and wake of freely falling cylinders at moderate Reynolds numbers. J. Fluid Mech. 866, 82–111.
Turton, R., Levenspiel, O., 1986. A short note on the drag correlation for spheres. Powder Technol. 47 (1), 83–86.
Veldhuis, C.H.J., Biesheuvel, A., 2007. An experimental study of the regimes of motion of spheres falling or ascending freely in a Newtonian fluid. Int. J. Multiph. Flow. 33 (10), 1074–1087.
Veldhuis, C.H.J., Biesheuvel, A., Lohse, D., 2009. Freely rising light solid spheres. Int. J. Multiph. Flow. 35 (4), 312–322.
Veldhuis, C.H.J., Biesheuvel, A., van Wijngaarden, L., Lohse, D., 2004. Motion and wake structure of spherical particles. Nonlinearity 18 (C1).
Will, J.B., Krug, D., 2021a. Dynamics of freely rising spheres: the effect of moment of inertia. J. Fluid Mech. 927, A7/1–20.
Will, J.B., Krug, D., 2021b. Rising and sinking in resonance: Mass distribution critically affects buoyancy-driven spheres via rotational dynamics. Phys. Rev. Lett. 126 (17), 174502.
Zhou, W., Dušek, J., 2015. Chaotic states and order in the chaos of the paths of freely falling and ascending spheres. Int. J. Multiph. Flow. 75, 205–223.